PNAS

Supporting Information for

Ionizing Radiation Exposure on Arrokoth Shapes a Sugar World

Chaojiang Zhang[1,2], Vanessa Leyva[3], Jia Wang[1,2], Andrew M. Turner[1,2], Mason Mcanally[1,2], Ashanie Herath[1,2], Cornelia Meinert [3]*, Leslie A. Young [4]*, Ralf I. Kaiser[1,2]*

[1] Department of Chemistry, University of Hawaii at Mānoa, Honolulu, HI 96822

[2] W.M. Keck Laboratory in Astrochemistry, University of Hawaii at Mānoa, Honolulu, HI 96822

[3] Université Côte d'Azur, Institut de Chimie de Nice, UMR 7272 CNRS, 06108 Nice, France

[4]Department of Space Studies, Southwest Research Institute, Boulder, CO 80302, USA.

*Corresponding authors:

Cornelia.MEINERT@univ-cotedazur.fr, layoung@boulder.swri.edu, ralfk@hawaii.edu.

This PDF file includes:

Figs. S1 to S19

Tables S1 to S14

SI References

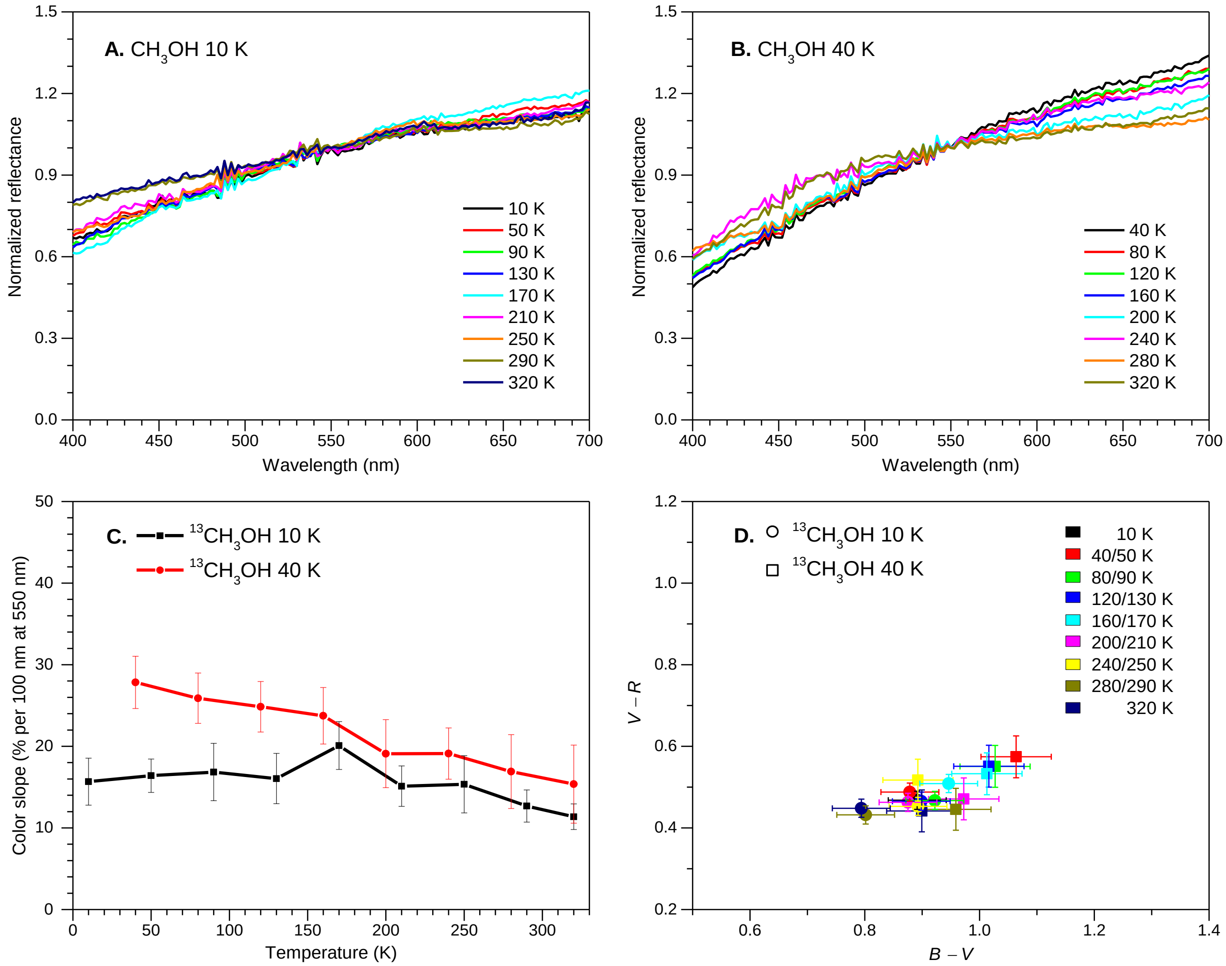

Fig. S1. Visible reflectance spectra and color of irradiated methanol ice during warming up to 320 K. (**A**) Spectra of methanol ice irradiated at 10 K and (**B**) 40 K. (**C**) Color slope evolution of irradiated methanol ice. (**D**) The color distribution of irradiated methanol ice. The irradiation at 10 K is coded with the circles and at 40 K was coded with the squares, the different temperatures are coded with different colors.

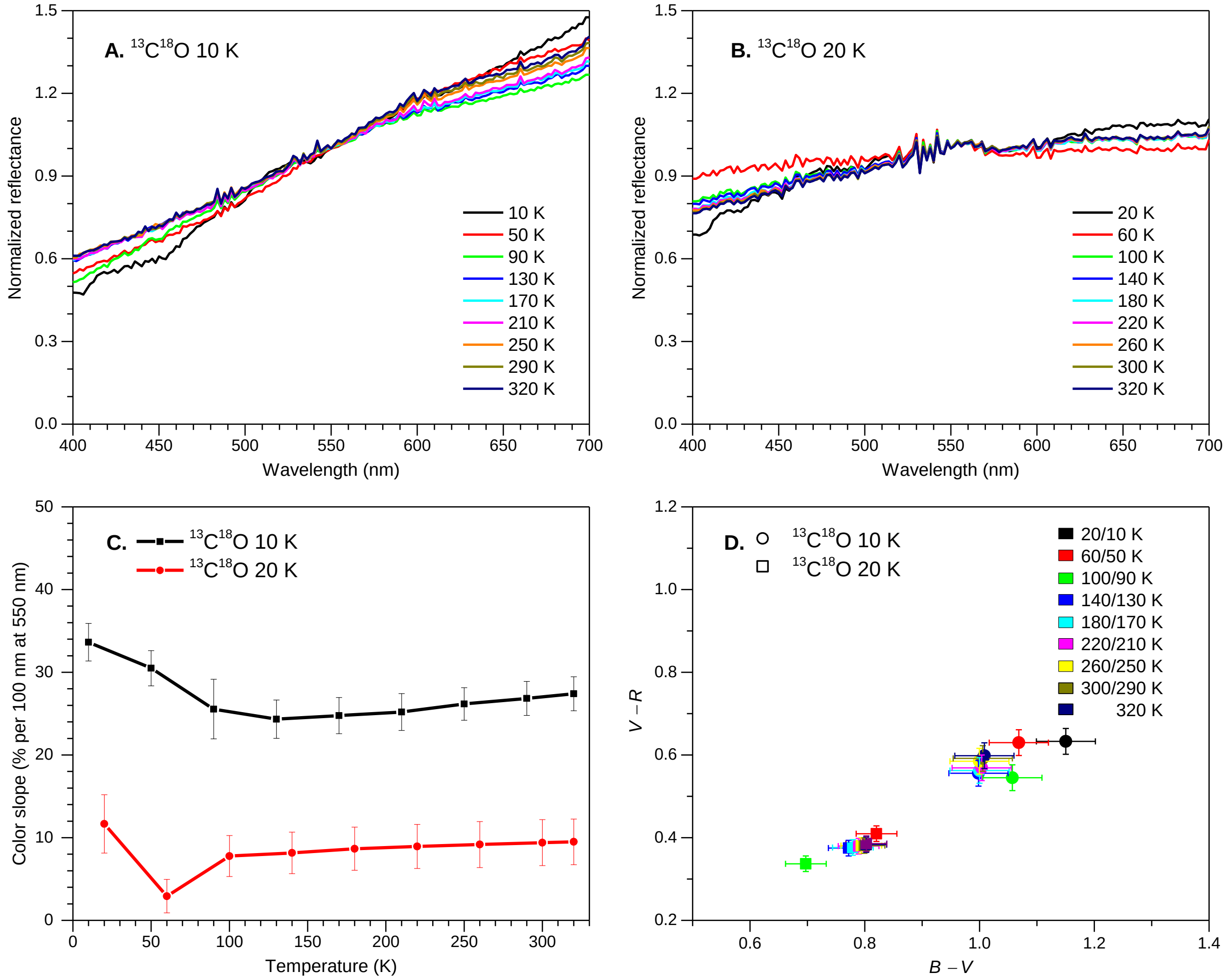

Fig. S2. Visible reflectance spectra and color of irradiated carbon monoxide ice during warming up to 320 K. (**A**) Spectra of carbon monoxide ice irradiated at 10 K, and (**B**) 20 K. (**C**) Color slope evolution of irradiated carbon monoxide ice. (**D**) The color distribution of irradiated carbon monoxide ice. The irradiation at 10 K is coded with the circles and at 20 K was coded with the squares, the different temperatures are coded with different colors.

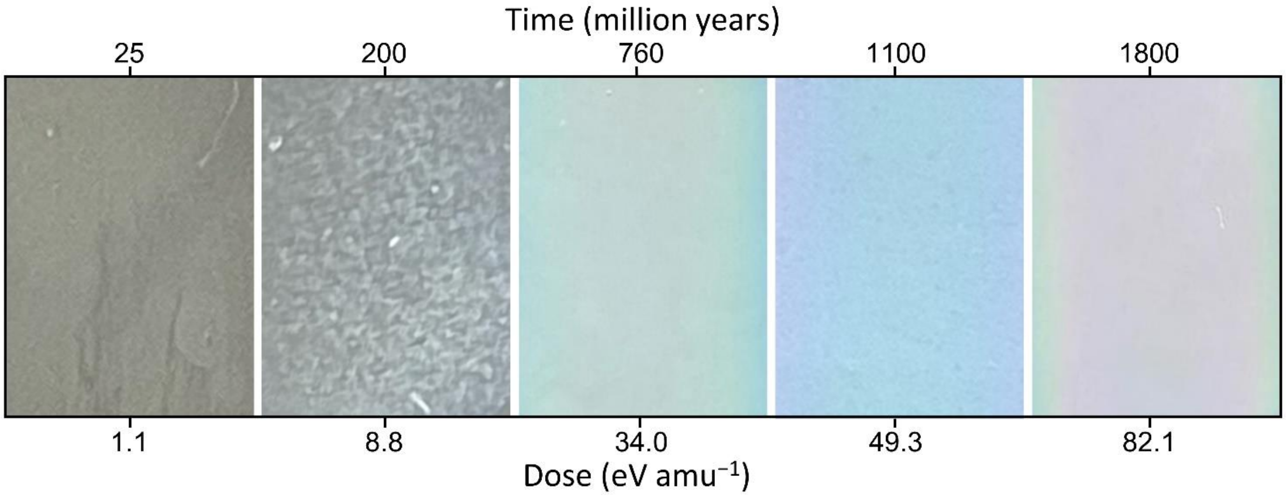

Fig. S3. Images of the residues for methanol ($^{13}CH_3OH$) ices irradiated at 40 K at distinct doses were recorded after annealing the ices to 320 K. These images were taken by a normal camera under the same conditions.

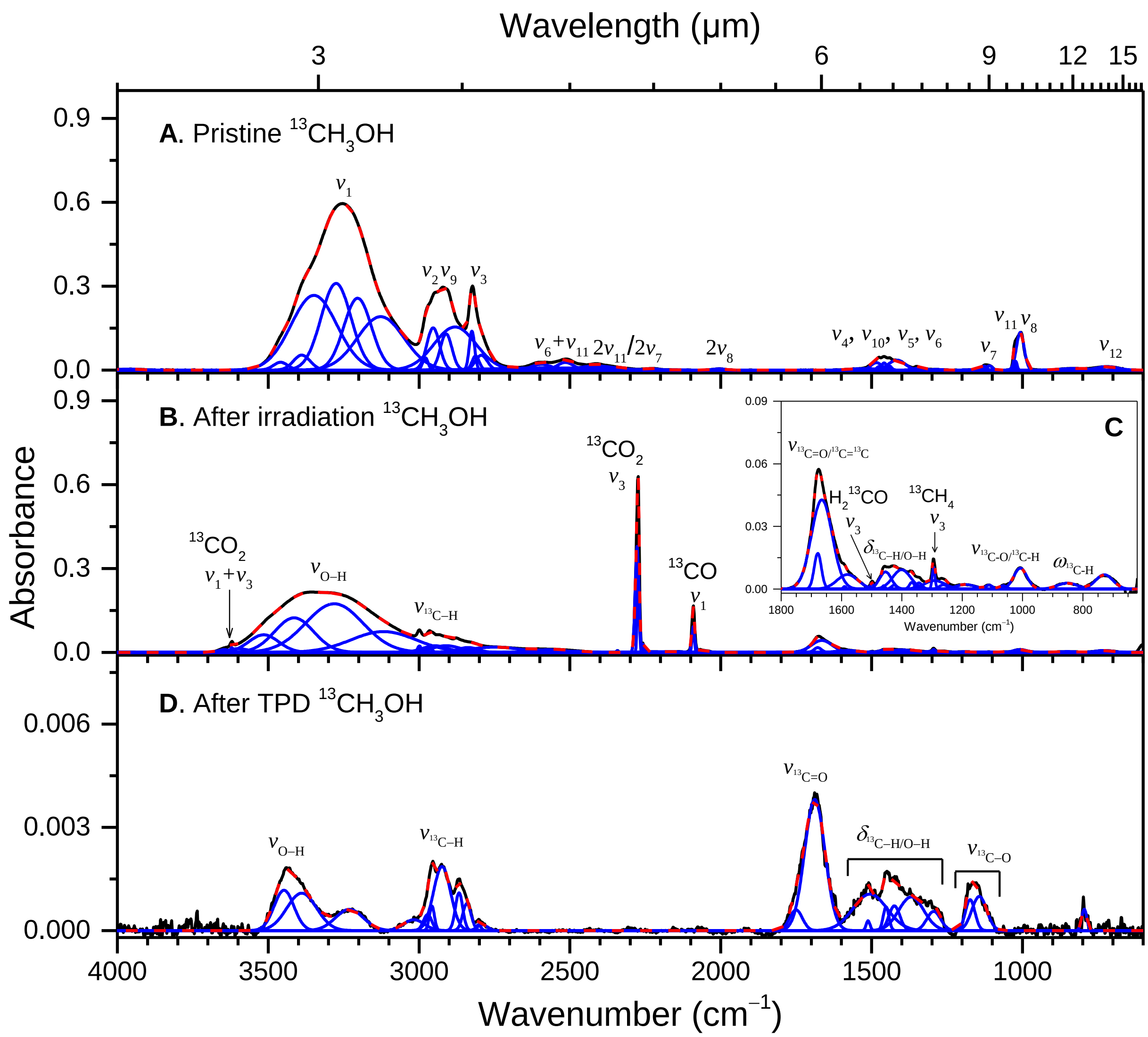

Fig. S4. Deconvoluted Fourier transform infrared spectra of methanol ice irradiated at 10 K. (**A**) Pristine ices at 10 K. (**B**) After irradiation at 10 K. (**C**) The magnified view of the region 1800–620 cm^{-1} of methanol ice after irradiation at 10 K. (**D**) The residue at 320 K. The experimental spectrum is plotted in black, while the deconvoluted peaks are blue and their sum is shown with the dashed red line. For clarity, only significant peaks are labeled, detailed peak assignments are listed in Table S4.

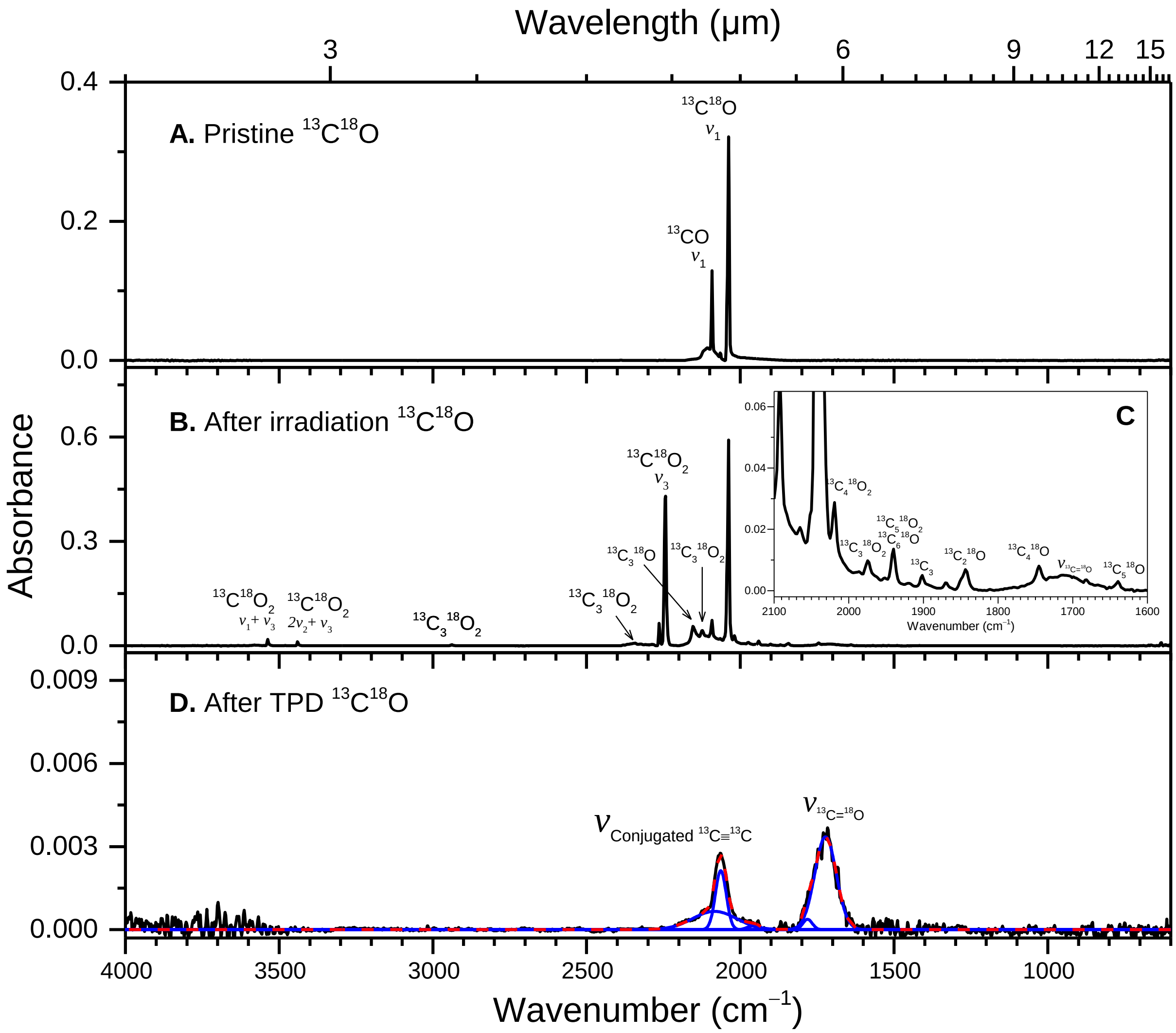

Fig. S5. Fourier transform infrared spectra of carbon monoxide ice irradiated at 10 K. (**A**) Pristine ices at 10 K. (**B**) After irradiation at 10 K. (**C**) The zoomed view of the region 2100–1600 cm^{-1} of carbon monoxide ice after irradiation at 10 K. (**D**) The residue at 320 K. The experimental spectrum is plotted in black, while the deconvoluted peaks are blue and their sum is shown with the dashed red line. For clarity, only significant peaks are labeled, and detailed peak assignments are listed in Table S6.

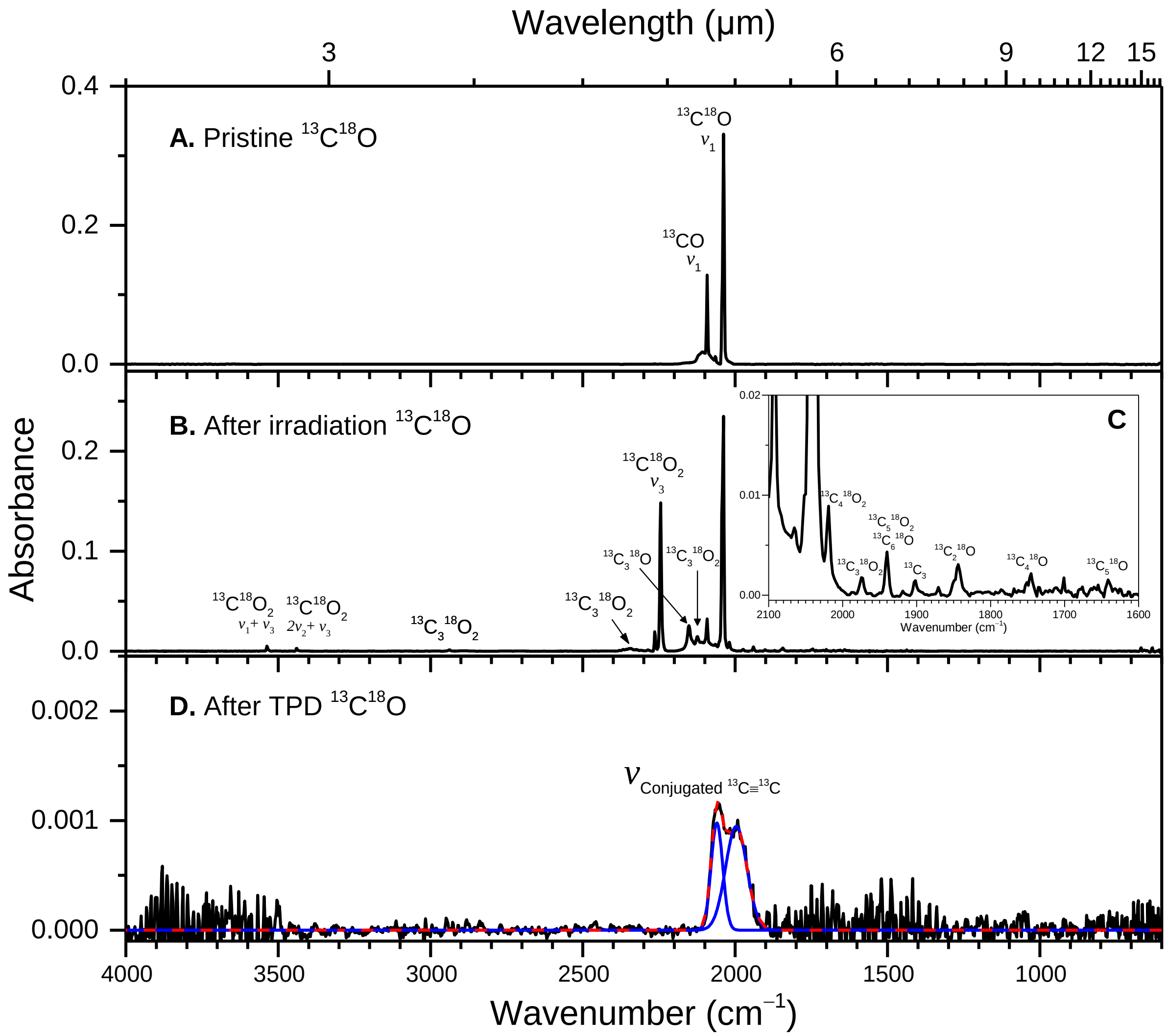

Fig. S6. Fourier transform infrared spectra of carbon monoxide ice irradiated at 20 K. (**A**) Pristine ices at 20 K. (**B**) After irradiation at 20 K. (**C**) The zoomed view of the region 2100–1600 cm^{-1} of carbon monoxide ice after irradiation at 20 K. (**D**) The residue at 320 K. The experimental spectrum is plotted in black, while the deconvoluted peaks are blue and their sum is shown with the dashed red line. For clarity, only significant peaks are labeled, and detailed peak assignments are listed in Table S7.

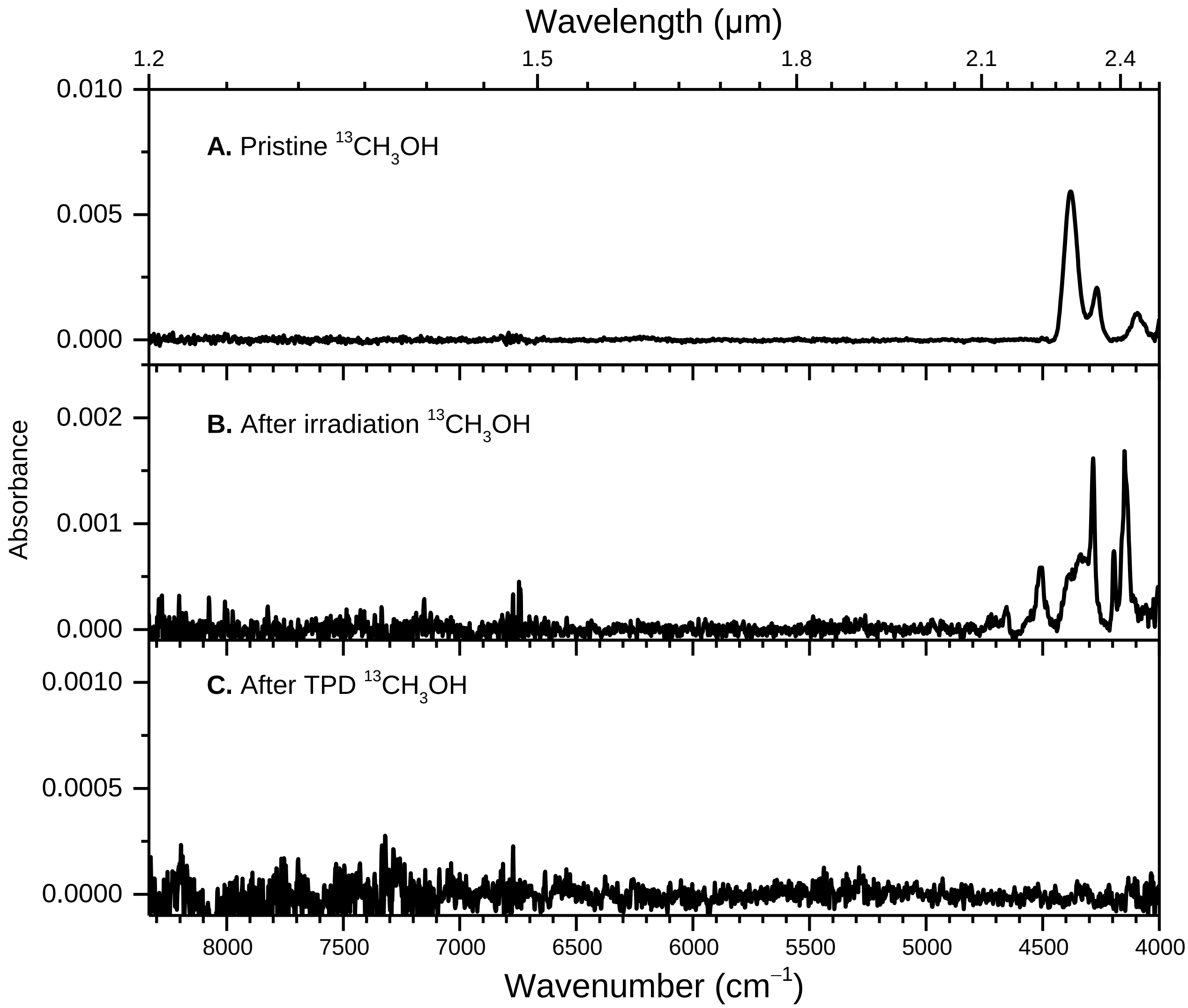

Fig. S7. Fourier transform infrared spectra of methanol ($^{13}CH_3OH$) recorded in the range of 4000–8333 cm^{-1}. (**A**) Pristine ices at 10 K. (**B**) After irradiation at 10 K. (**C**) Residue at 320 K. Detailed peak assignments are compiled in Table S4.

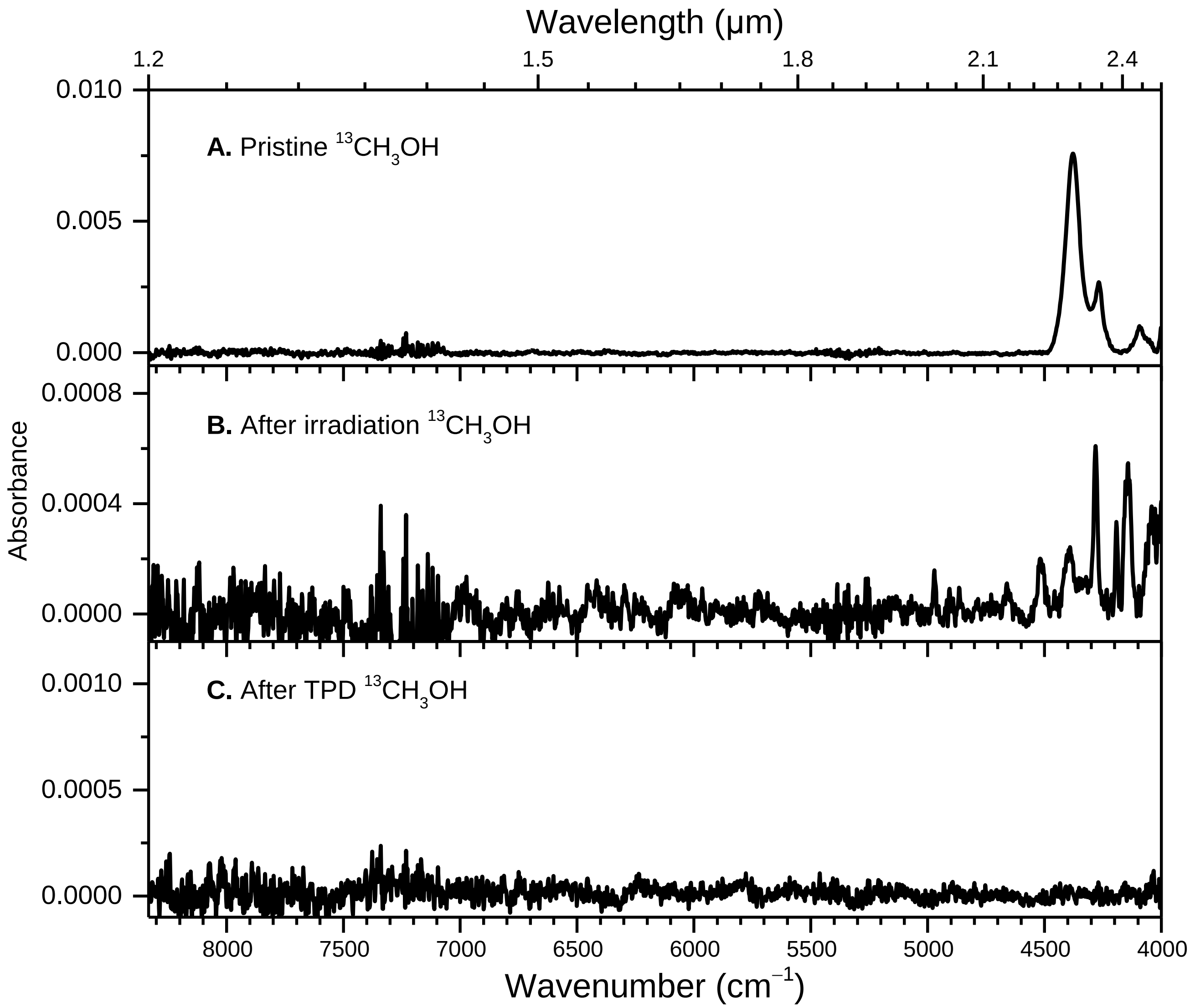

Fig. S8. Fourier transform infrared spectra of methanol ($^{13}CH_3OH$) recorded in the range of 4000–8333 cm^{-1}. (**A**) Pristine ices at 40 K. (**B**) After irradiation at 40 K. (**C**) Residue at 320 K. Detailed peak assignments are compiled in Table S5.

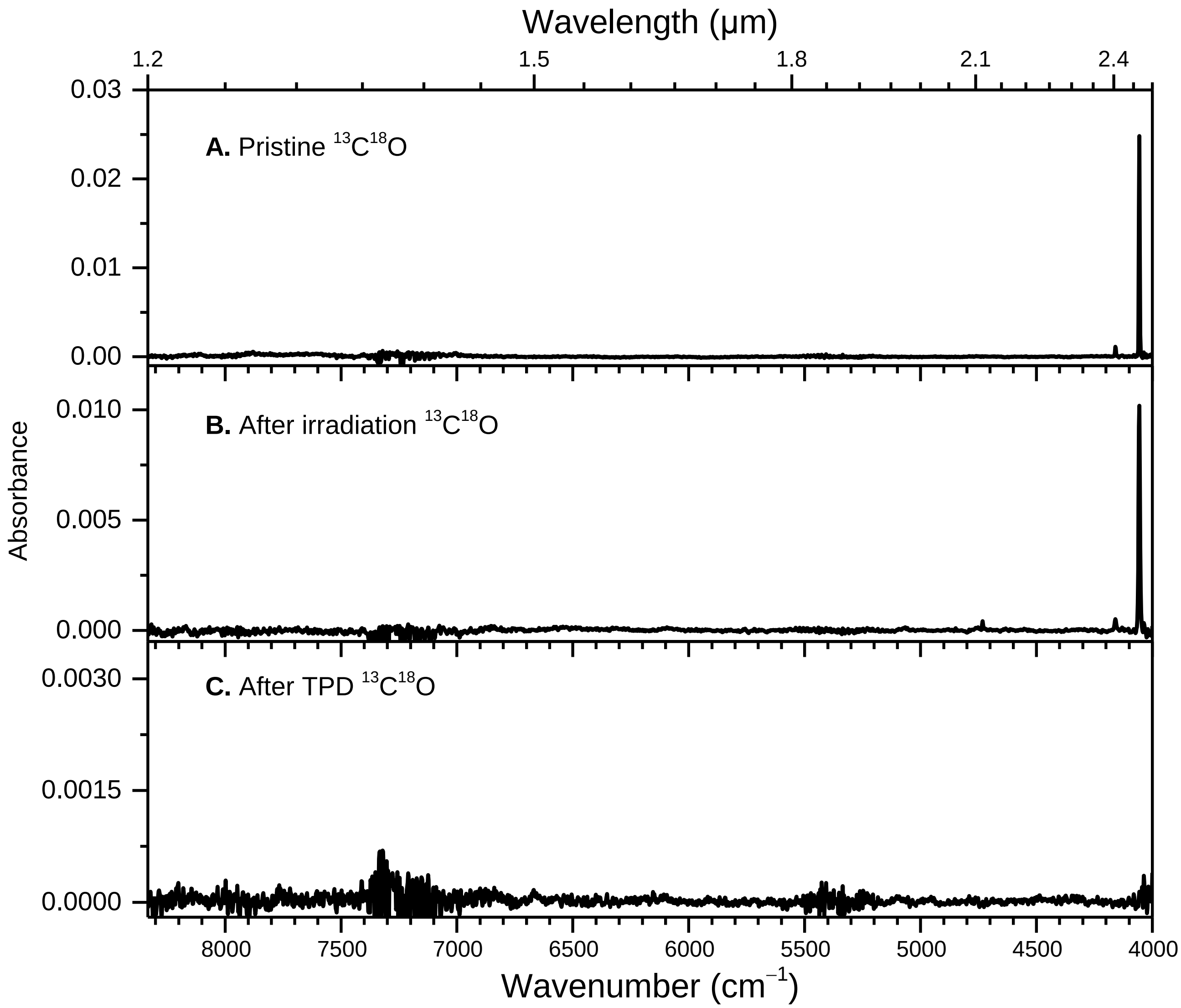

Fig. S9. Fourier transform infrared spectra of carbon monoxide ($^{13}C^{18}O$) recorded in the range of 4000–8333 cm^{-1}. (**A**) Pristine ices at 10 K. (**B**) After irradiation at 10 K. (**C**) Residue at 320 K. Detailed peak assignments are compiled in Table S6.

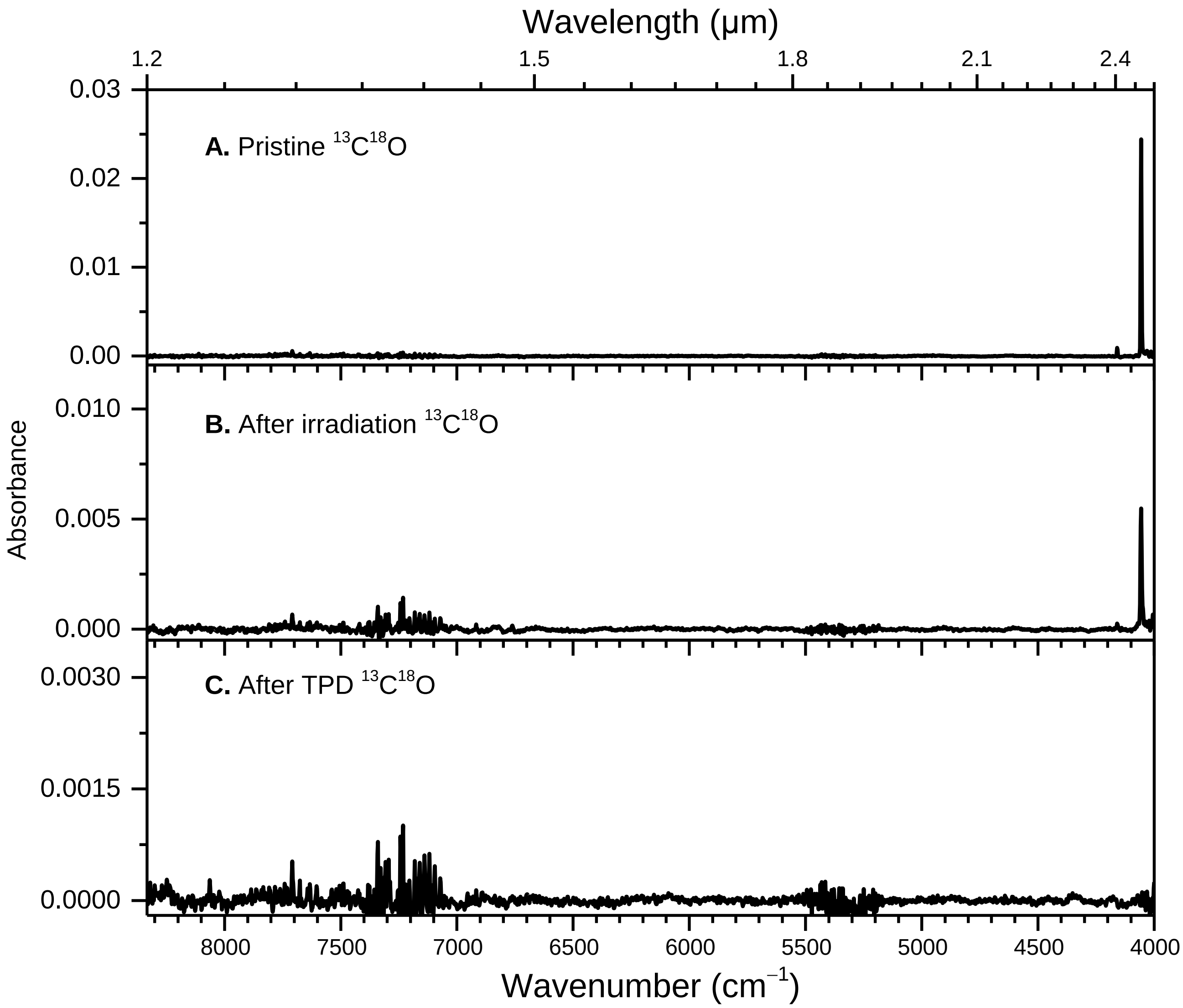

Fig. S10. Fourier transform infrared spectra of carbon monoxide ($^{13}C^{18}O$) recorded in the range of 4000–8333 cm^{-1}. (**A**) Pristine ices at 20 K. (**B**) After irradiation at 20 K. (**C**) Residue at 320 K. Detailed peak assignments are compiled in Table S7.

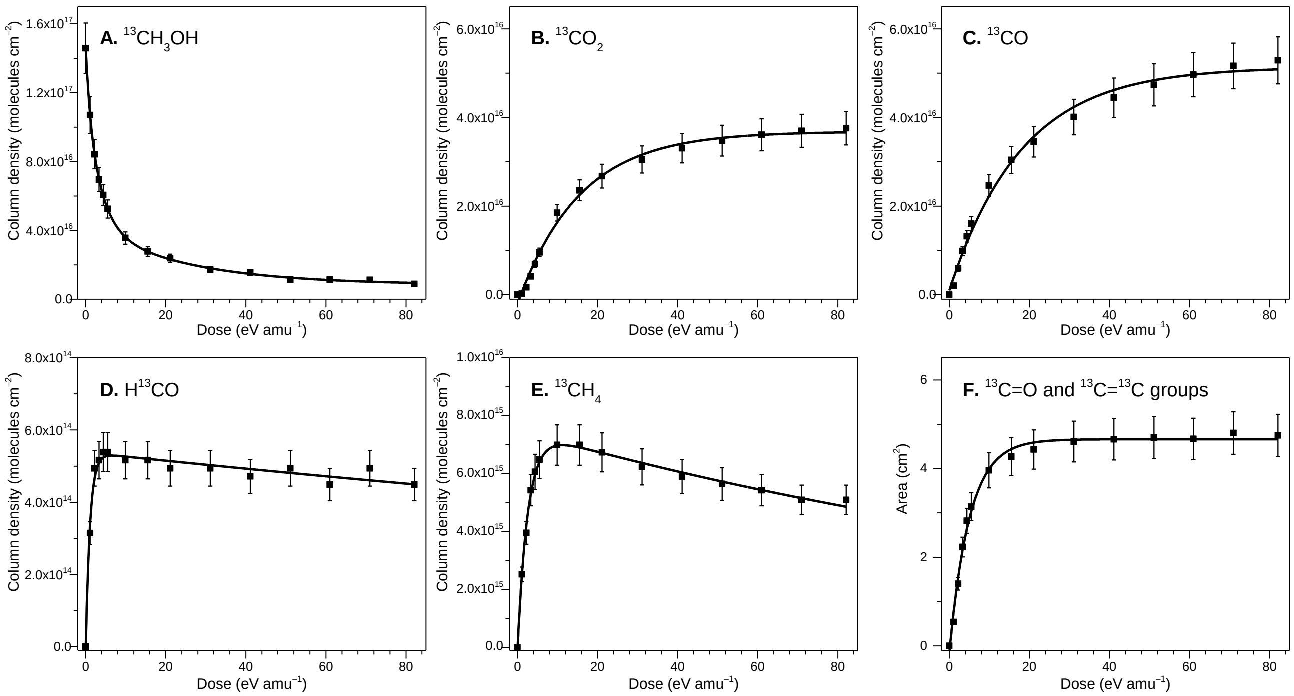

Fig. S11. The evolution and kinetic fits of key species and functional groups during the irradiation of methanol ($^{13}CH_3OH$) ice at 10 K. (**A**) Column densities of methanol ($^{13}CH_3OH$, average of 1124 cm^{-1} and 1105 cm^{-1}). (**B**) Column densities of carbon dioxide ($^{13}CO_2$, 2275 cm^{-1}). (**C**) Column densities of carbon monoxide (^{13}CO, 2091 cm^{-1}). (**D**) Column densities of formyl radical ($H^{13}CO$, 1805 cm^{-1}). (**E**) Column densities of methane ($^{13}CH_4$, 1294 cm^{-1}). (**F**) Area of $^{13}C=O$ and $^{13}C=^{13}C$ stretch group (band between 1520–1790 cm^{-1}). All the error bars are ±10% of the corresponding column densities and areas. Rate constants derived from the kinetic fitting and corresponding chemical reaction scheme are compiled in Table S8.

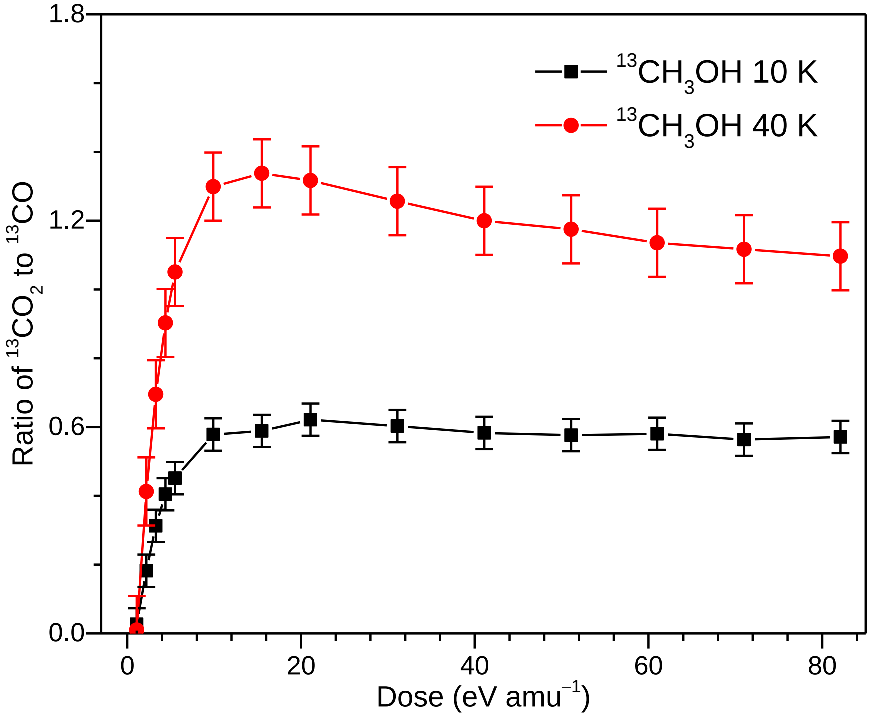

Fig. S12. The evolution of carbon dioxide ($^{13}CO_2$) to carbon monoxide (^{13}CO) ratio during the irradiation of methanol ices.

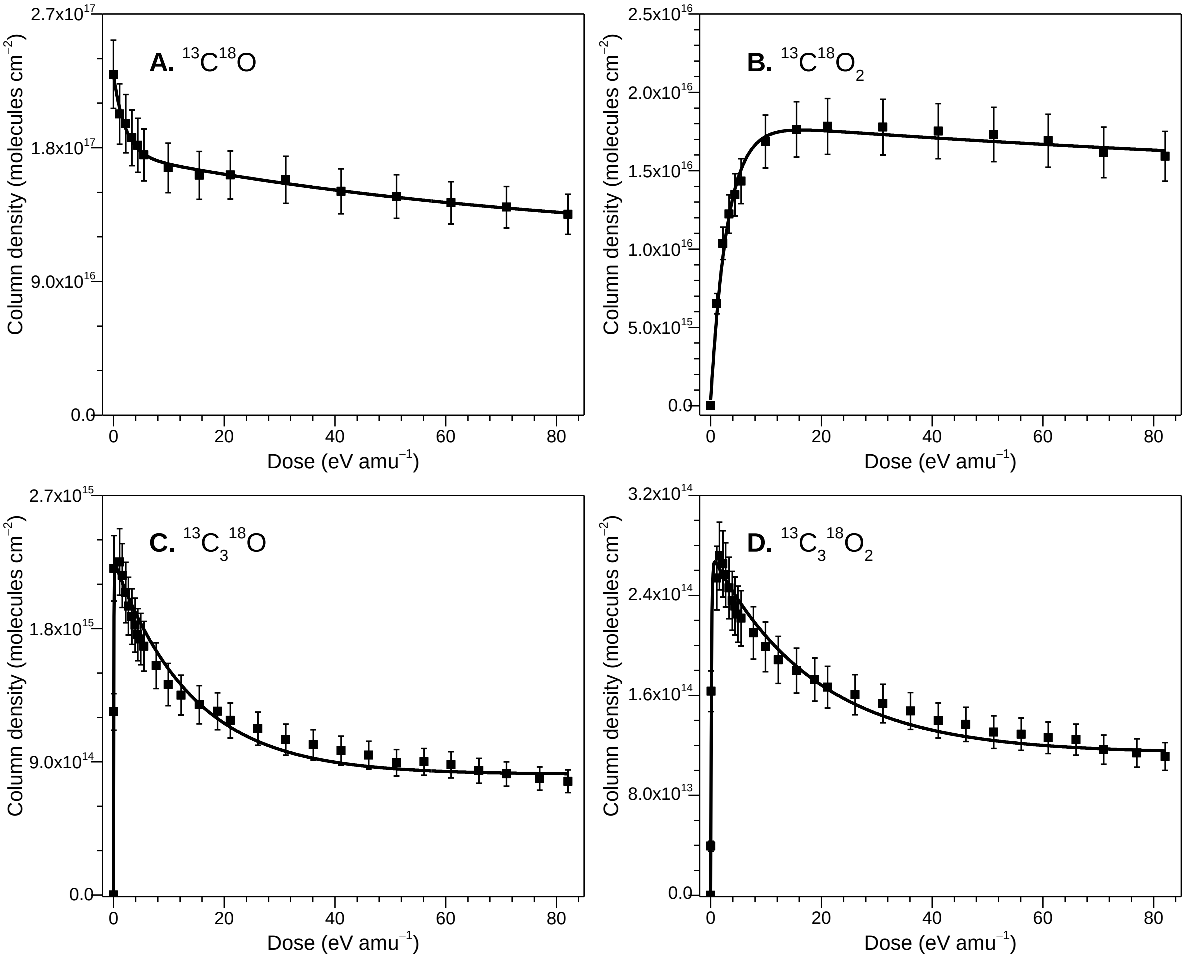

Fig. S13. The evolution and kinetic fits of representative species during the irradiation of carbon monoxide ($^{13}C^{18}O$) ice at 10 K. (**A**) Carbon monoxide ($^{13}C^{18}O$, 4055 cm^{-1}). (**B**) Carbon dioxide ($^{13}C^{18}O_2$, 2244 cm^{-1}). (**C**) Tricarbon monoxide ($^{13}C_3{}^{18}O$, 2153 cm^{-1}). (**D**) Carbon suboxide ($^{13}C_3{}^{18}O_2$, 2123 cm^{-1}). Error bars shown are 1σ values. All the error bars are ±10% of the corresponding column densities. Rate constants derived from the kinetic fitting and the corresponding chemical reaction scheme are compiled in Table S9.

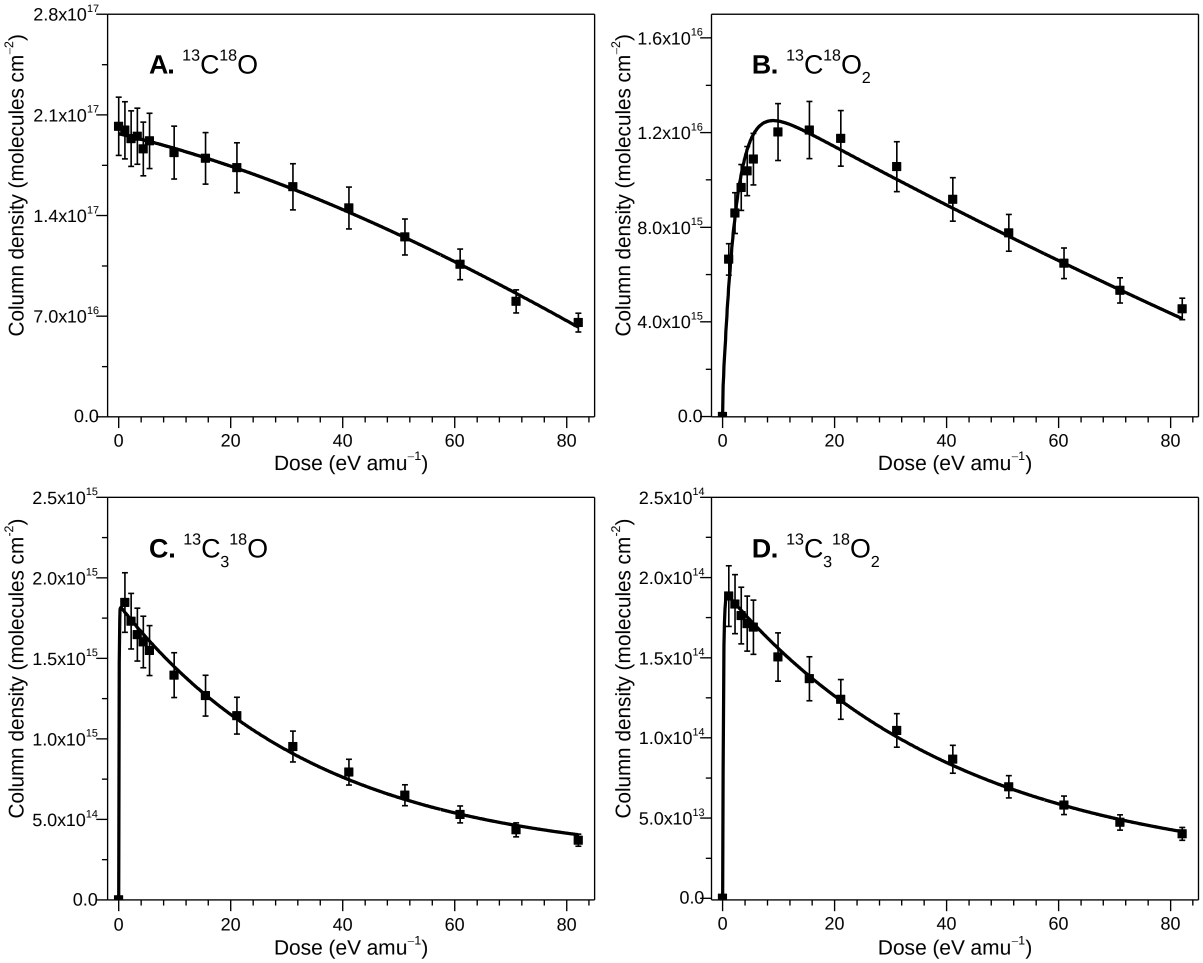

Fig. S14. The evolution and kinetic fits of representative species during the irradiation of carbon monoxide ($^{13}C^{18}O$) ice were irradiated at 20 K. (**A**) Carbon monoxide ($^{13}C^{18}O$, 4055 cm^{-1}). (**B**) Carbon dioxide ($^{13}C^{18}O_2$, 2244 cm^{-1}). (**C**) Tricarbon monoxide ($^{13}C_3{}^{18}O$, 2153 cm^{-1}). (**D**) Carbon suboxide ($^{13}C_3{}^{18}O_2$, 2123 cm^{-1}). All the error bars are ±10% of the corresponding column densities. Rate constants derived from the kinetic fitting and the corresponding chemical reaction scheme are compiled in Table S9.

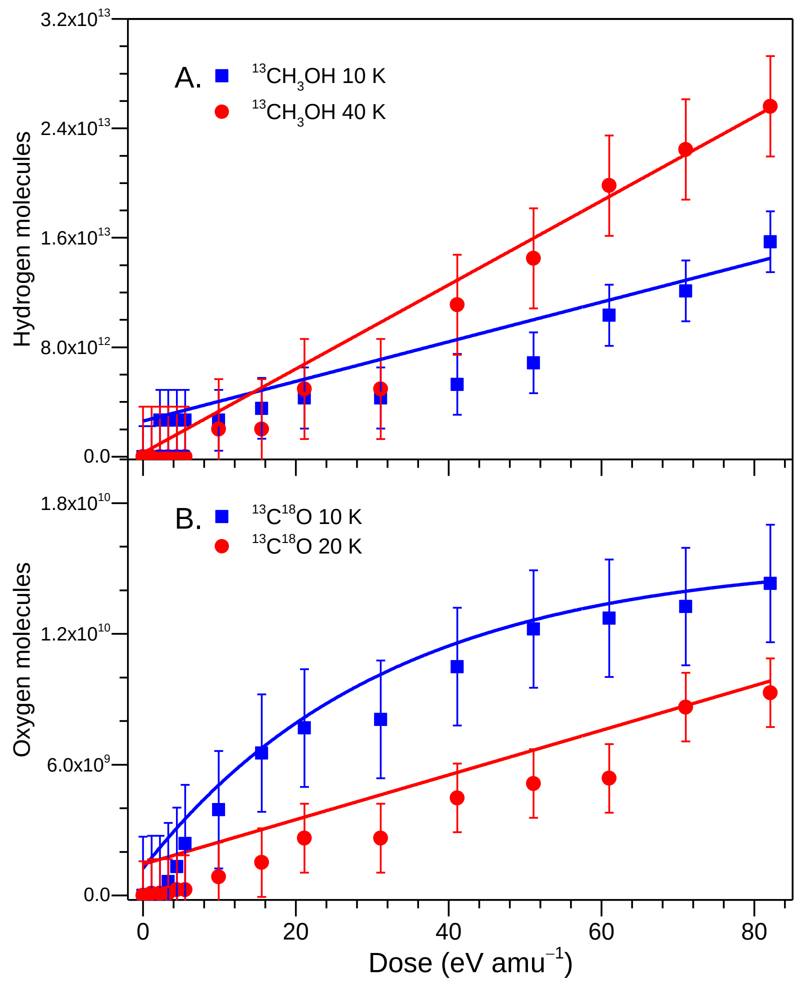

Fig. S15. Counts of molecules detected by quadrupole mass spectrometry QMS. (**A**) Molecular hydrogen (H_2, *m/z* = 2) from irradiated methanol ($^{13}CH_3OH$) ice. The molecular hydrogen counts are (2.9 ± 0.3) × 10^{15} for methanol ice irradiated at 10 K and (1.0 ± 0.1) × 10^{15} for methanol ice irradiated at 40 K during warmed up to 320 K, respectively. (**B**) Molecular oxygen ($^{18}O_2$, *m/z* = 36) form irradiated carbon monoxide ($^{13}C^{18}O$) ice. The molecular oxygen counts are (3.4 ± 0.3) × 10^{12} for carbon monoxide ice irradiated at 10 K and (1.6 ± 0.2) × 10^{11} for carbon monoxide ice irradiated at 20 K during warmed up to 320 K, respectively.

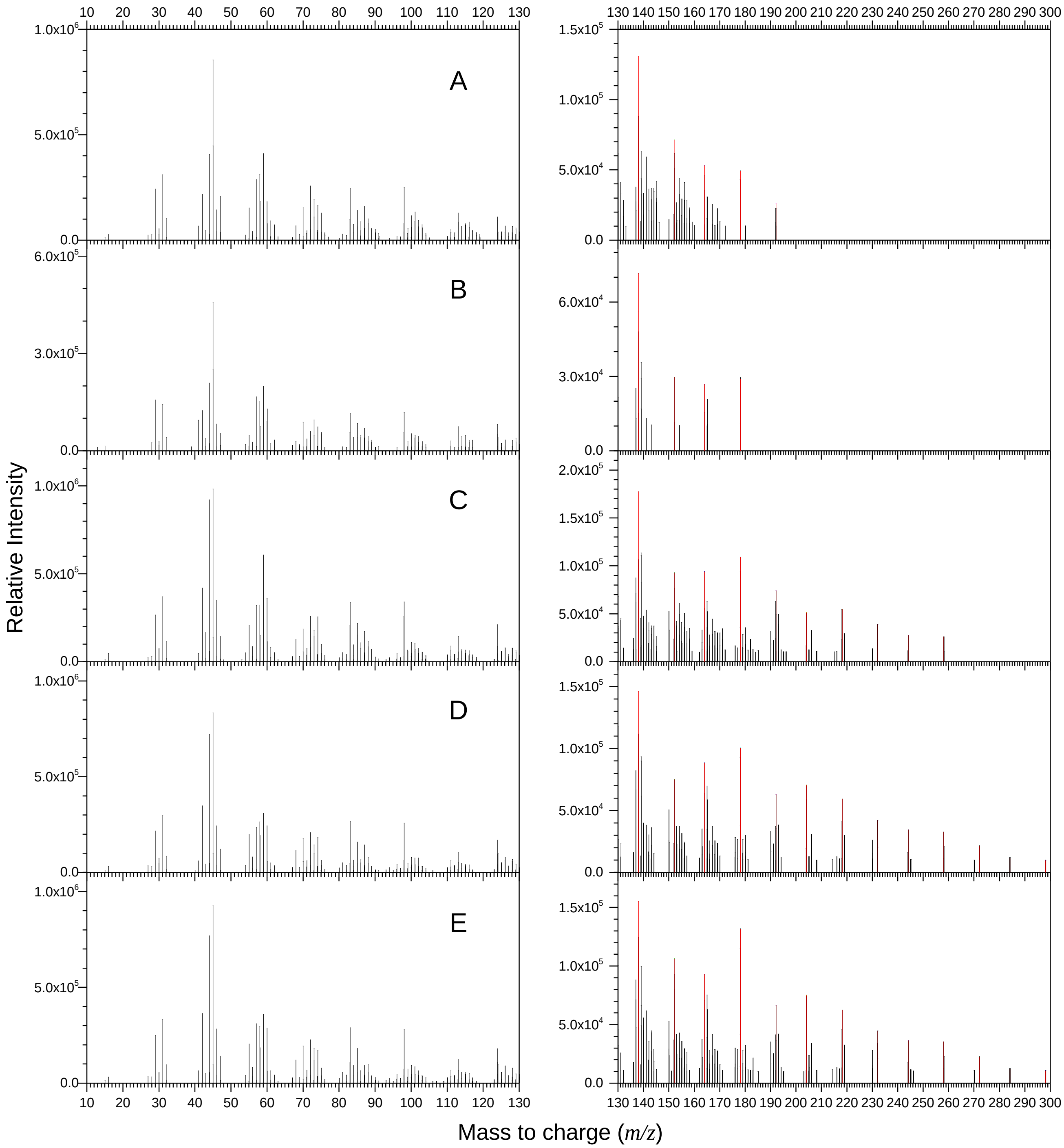

Fig. S16. Dominant positive ion SIMS data of the residues from methanol ($^{13}CH_3OH$) irradiated at 40 K. The data were recorded in the mass to charge from 10 to 150 (left) and mass to charge from 150 to 300 (right) correlated with (**A**) 8.8 eV amu^{-1}, (**B**) 23.0 eV amu^{-1}, (**C**) 34.0 eV amu^{-1}, (**D**) 49.3 eV amu^{-1}, and (**E**) 82.1 eV amu^{-1}. Red vertical lines are signals of polycyclic aromatic hydrocarbons (PAHs) fragments.

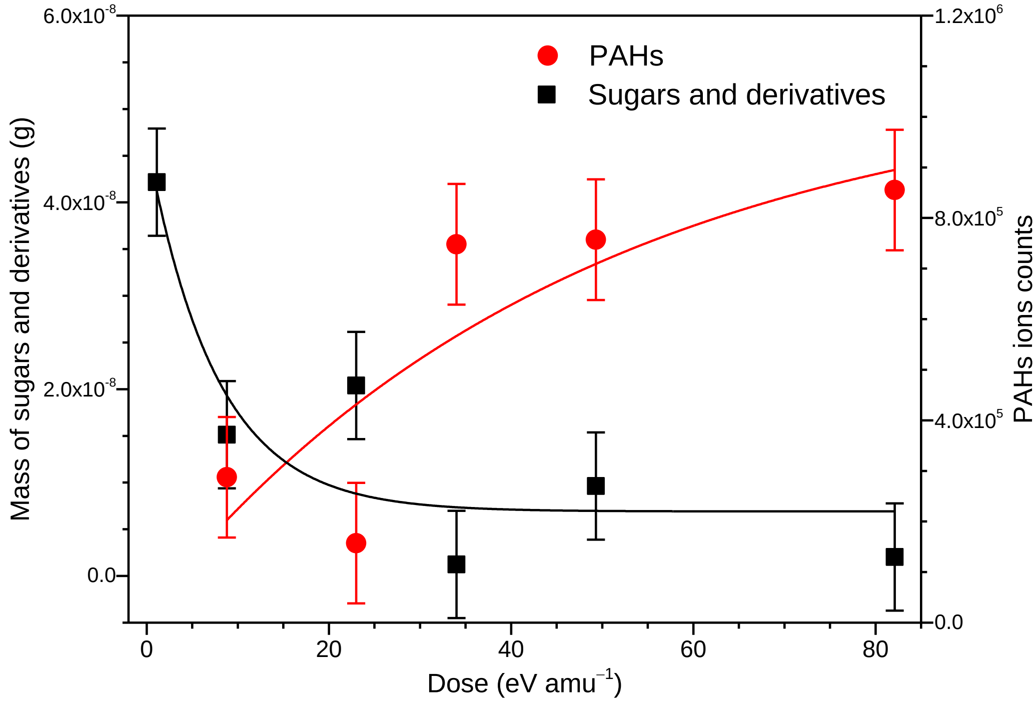

Fig. S17. The evolution of the mass of sugars and their derivatives and the changes of integrated counts of polycyclic aromatic hydrocarbons (PAHs) detected in the residues of irradiated methanol when extending irradiation time.

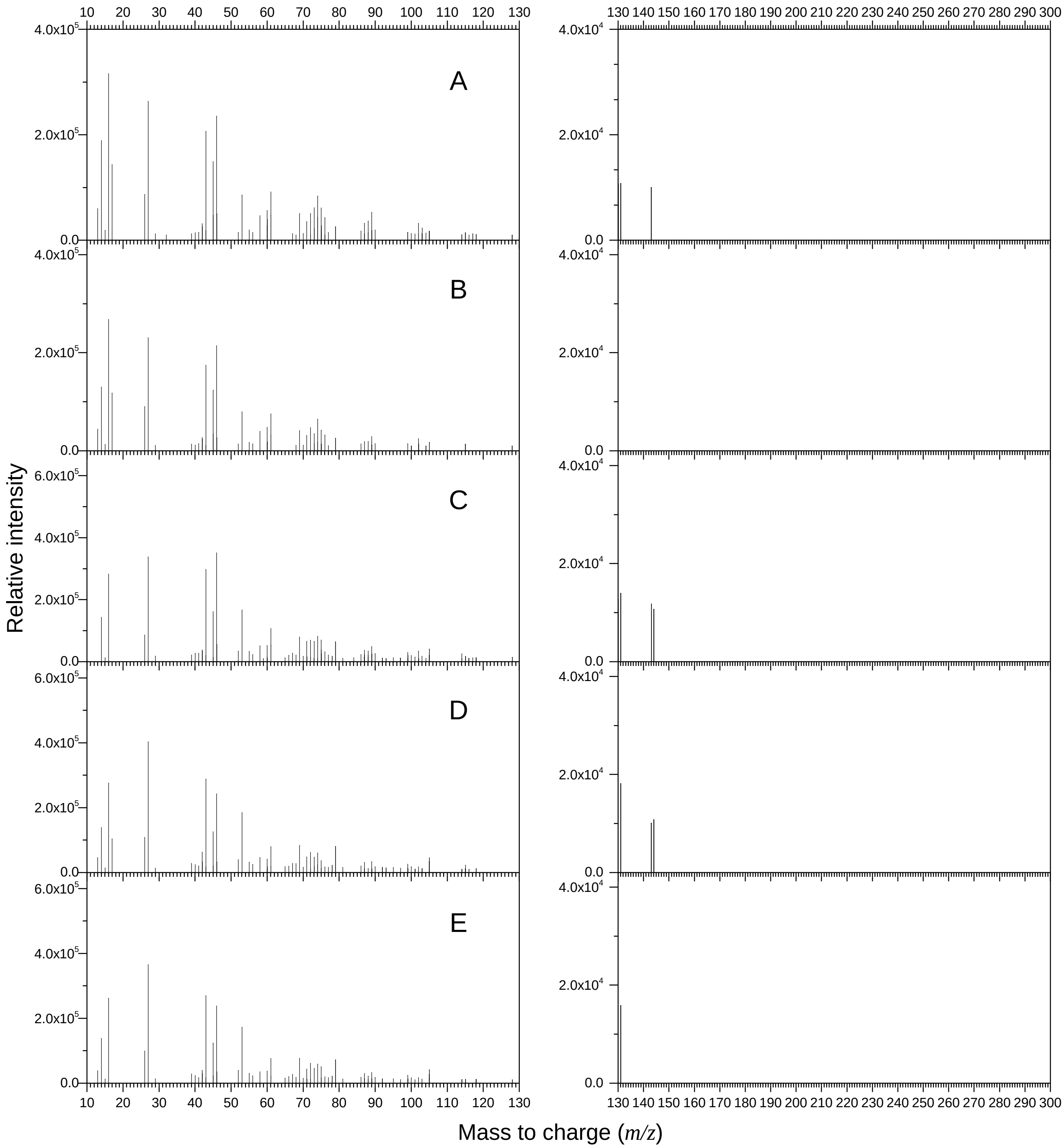

Fig. S18. Dominant negative ion SIMS data of the residues from methanol ($^{13}CH_3OH$) irradiated at 40 K. The data were recorded in the mass to charge from 10 to 150 (left) and mass to charge from 150 to 300 (right) correlated with (**A**) 8.8 eV amu^{-1}, (**B**) 23.0 eV amu^{-1}, (**C**) 34.0 eV amu^{-1}, (**D**) 49.3 eV amu^{-1}, and (**E**) 82.1 eV amu^{-1}.

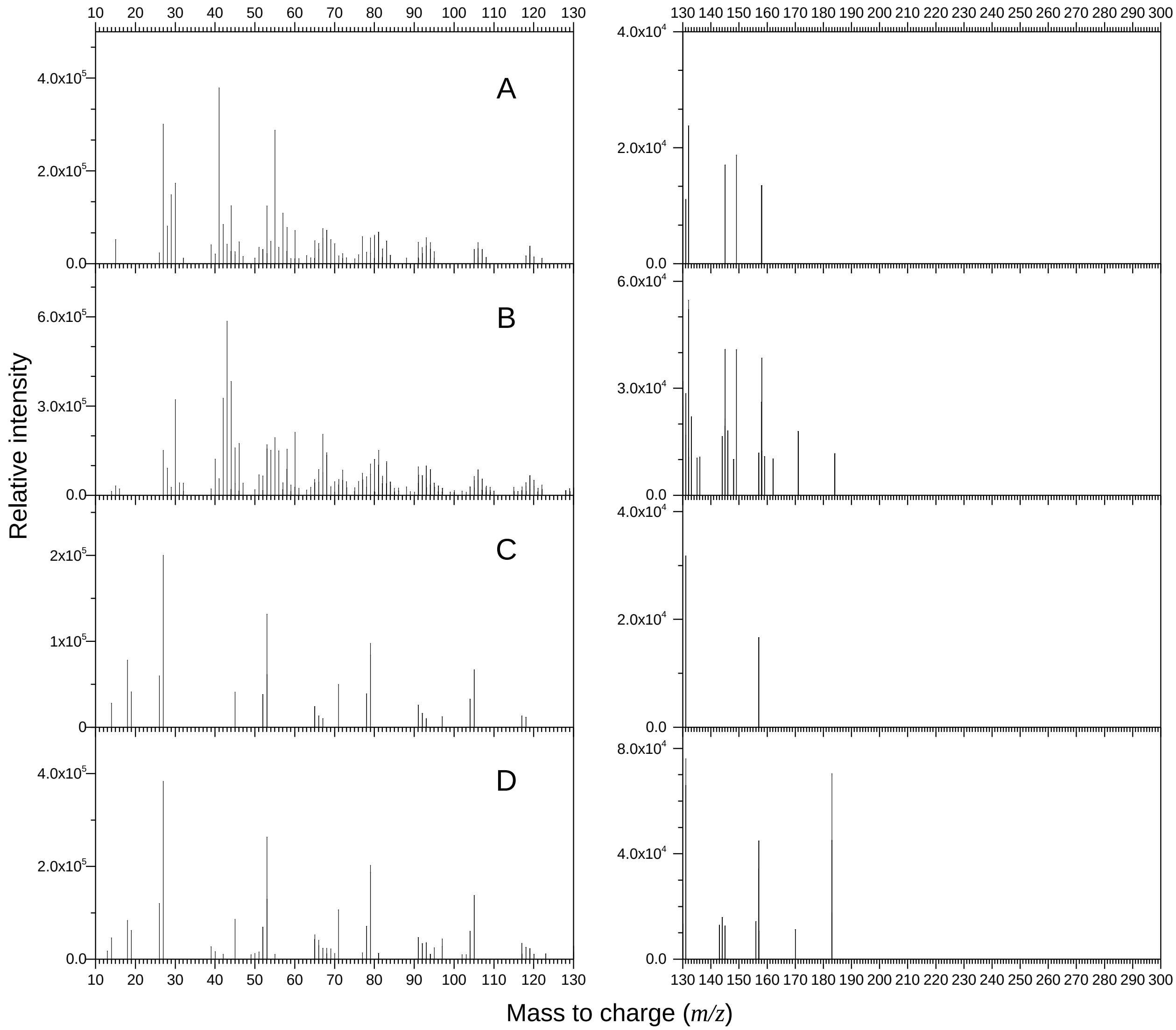

Fig. S19. Dominant SIMS data of the residues from carbon monoxide ($^{13}C^{18}O$) irradiated at 10 and 20 K with a dose of 82.1 eV amu^{-1}. The data were recorded in the mass to charge from 10 to 150 (left) and mass to charge from 150 to 300 (right) correlated with (**A**) positive signal of carbon monoxide ($^{13}C^{18}O$) irradiated at 10 K, (**B**) positive signal of carbon monoxide ($^{13}C^{18}O$) irradiated at 20 K, (**C**) negative signal of carbon monoxide ($^{13}C^{18}O$) irradiated at 10 K, and (**D**) negative signal of carbon monoxide ($^{13}C^{18}O$) irradiated at 20 K.

Table S1. Compilation of the identified sugars and related compounds in meteorites, the interstellar medium (ISM), and methanol-containing interstellar analogous ices.

	Compound	Formula	References		
			Meteorites	ISM	Methanol−containing ices
Sugars	Glycolaldehyde	CH_2OHCHO		(1)	(2-5)
	Glyceraldehyde	CH_2OHCH_2OHCHO			(5)
	Dihydroxyacetone	$CH_2OHCOCH_2OH$	(6)		(5)
	Erythrose, α-furanose	$CH_2OH(CHOH)_2CHO$			(5)
	Erythrulose	$CH_2OHCHOHCOCH_2OH$			(5)
	Arabinose, Ribose, Xylose, Lyxose	$CH_2OH(CHOH)_3CHO$	(6)		(5, 7)
Sugar alcohols	Ethylene glycol	CH_2OHCH_2OH	(8)	(9)	(5, 10-13)
	1, 3-Propanediol	$CH_2OHCH_2CH_2OH$			(5, 7, 11)
	1, 2-Propanediol	$CH_2OHCH_2OHCH_3$	(14)		
	Glycerol	$HOCH_2CHOHCH_2OH$	(8, 15)		(5, 11, 13, 16)
	1,3-Butanediol	$HOCH_2CH_2CHOHCH_2$			(11)
	2-Methyl glycerol	$HOCH_2COH(CH_3)CH_2OH$			(5)
	Erythritol & Threitol	$HOCH_2(CHOH)_2CH_2OH$	(8, 15)		(5)
	2-Hydroxymethyl glycerol	$(HOCH_2)_2C(OH)CH_2OH$	(8, 15)		(5)
	Ribitol, Arabinitol, Xylitol	$HOCH_2(CHOH)_3CH_2OH$	(8, 15)		(5)
	Mannitol, Sorbitol, Allitol, Dulcitol, Talitol	$HOCH_2(CHOH)_4CH_2OH$	(8, 15)		(5)
Sugar acids	Glyceric acid	$HOCH_2(CHOH)COOH$	(8, 15)		(11) (5)
	Erythronic acid, Threonic acid	$HOCH_2(CHOH)_2COOH$	(8, 15)		(5)
	Ribonic, Arabinonic, Xylonic, Lyxonic,	$HOCH_2(CHOH)_3COOH$	(8, 15)		(5)
	Allonic, Altronic, Gluconic, Mannonic, Gulonic, Idonic, Galactonic, Talonic	$HOCH_2(CHOH)_4COOH$	(8)		

Table S1. *continued*

	Compound	Formula	References		
			Meteorites	ISM	Methanol−containing ices
Hydroxy-carboxylic acids	Glycolic acid	$HOCH_2COOH$			(5, 10, 11, 17)
	Lactic acid	$CH_3CH(OH)COOH$	(14)		(5)
	3-Hydroxypropionic acid	$HOCH_2CH_2COOH$			(5), (11)
	2-Hydroxybutyric acid	$CH_3CH_2CH(OH)COOH$	(14)		(5)
	2-Hydroxyisobutyric acid	$(CH_3)_2C(OH)COOH$	(14)		(5)
	3-Hydroxybutyric acid	$CH_3CH(OH)CH_2COOH$	(14)		(11)
	3-Hydroxyisobutyric acid	$CH_3CH(CH_2OH)COOH$	(14)		(5)
	4-Hydroxybutyric acid	$HOCH_2CH_2CH_2COOH$	(14)		(5, 11)
	2-Hydroxylmethyl glyceric acid (HMT)	$(HOCH_2)_2COHCOOH$	(8, 15)		
	2-Methyl glyceric acid	$HOCH_2C(CH_3)(OH)COOH$	(8, 15)		(5)
	2, 4-Dihydroxybutyric acid	$HOCH_2CH_2CH(OH)COOH$	(8, 15)		
	2, 3-Dihydroxybutyric acid	$CH_3(CHOH)_2COOH$	(8, 15)		
	3, 4-Dihydroxybutyric acid	$HOCH_2CH(OH)CH_2COOH$	(8, 15)		(7)
	2-Deoxy-pentonic acids	$HOOCHCH_2(CHOH)_2COOH$	(15)		
	Malic acid	$HOOCHCH_2CHOHCOOH$	(14)		(5)
Dihydroxy-carboxylic acids	Malonic acid	$HOOCHCH_2COOH$			(5)
	Succinic acid	$HOOCH(CH_2)_2COOH$			(5)
	Fumaric acid	HOOCHCH=CH COOH			(5)
	Tartaric acid, Mesotartaric acid	$HOOCH(CHOH)_2COOH$	(15)		
Deoxysugar	2-Deoxy-ribose, 2-Deoxy-xylose	$CH_2OH(CHOH)_2CH_2CHO$			(7)

Table S2. Data applied to calculate the average irradiation dose on ice surface.

Initial kinetic energy of the electrons, E_{init} (keV)	5	
Ice	$^{13}CH_3OH$	$^{13}C^{18}O$
Irradiation current, I (nA)	1300 ± 120	1300 ± 120
Total number of electrons	2.92×10^{17}	2.92×10^{17}
Average penetration depth, l (nm)[a]	230 ± 30	270 ± 30
Average kinetic energy of backscattered electrons, E_{bs} (eV)[a]	3170 ± 320	3430 ± 320
Fraction of backscattered electrons, f_{bs}[a]	0.3 ± 0.03	0.4 ± 0.03
Average kinetic energy of transmitted electrons, E_{trans} (eV)[a]	0	0
Fraction of transmitted electrons, f_{trans}[a]	0	0
Irradiated area, A (cm^2)	1 ± 0.05	1 ± 0.05
Dose (eV $molecule^{-1}$)	2710 ± 320	2550 ± 320
Dose (eV amu^{-1})	82.1 ± 10.0	

Note.
[a] Parameters obtained from CASINO software v2.4.

Table S3. The absorption coefficients used to estimate the column density of methanol and carbon monoxide ice and the radiation products identified in the Fourier transform infrared (FTIR) spectra (18-20).

Compound	Mode	Position (cm^{-1})	Absorption coefficients (cm $molecule^{-1}$)
Methanol ($^{13}CH_3OH$)	v_{11}	1005	1.07×10^{-17}
	v_7	1024	1.4×10^{-18}
Methane ($^{13}CH_4$)	v_3	1294	8.0×10^{-18}
Formyl radical ($H^{13}CO$)	v_2	1805	1.5×10^{-17}
Carbon dioxide(^{13}CO)	v_1	2091	1.12×10^{-17}
Carbon submonoxide ($^{13}C_3{}^{18}O_2$)	-	2123	4.7×10^{-16}
Tricarbon monoxide ($^{13}C_3{}^{18}O$)	-	2153	2.5×10^{-16}
Carbon monoxide ($^{13}CO_2$)	v_3	2275	7.6×10^{-17}

Table S4. Infrared absorption features of methanol ice ($^{13}CH_3OH$) irradiated at 10 K recorded before irradiation, after irradiation, and after TPD. Assignments based on references (11, 19, 21).

Before irradiation (cm^{-1})	After irradiation (cm^{-1})	After TPD (cm^{-1})	Assignment
	4511		$\nu_2 + \nu_3$ ($^{13}CH_4$)
4383	4383		$\nu_{2/9} + \nu_{4/6/10}$ ($^{13}CH_3OH$)
4273			$\nu_{2/9} + \nu_4$ ($^{13}CH_3OH$)
	4283		$\nu_3 + \nu_4$ ($^{13}CH_4$)
	4195		$2\nu_1$ (^{13}CO)
	4149		$\nu_1 + \nu_4$ ($^{13}CH_4$)
3955			$\nu_1 + \nu_{12}$ ($^{13}CH_3OH$)
	3620		$\nu_1 + \nu_{13}$ ($^{13}CO_2$)
	3646, 3600, 3517, 3414, 3278, 3114,	3446, 3388, 3230	O−H stretch
3460, 3391, 3350, 3275, 3207, 3129			ν_1 ($^{13}CH_3OH$)
2979, 2951,			ν_2 ($^{13}CH_3OH$)
2920, 2881			ν_9 ($^{13}CH_3OH$)
	2998, 2963, 2944, 2908, 2875, 2836, 2753, 2571, 2484	3019, 2995, 2925, 2902, 2866, 2839, 2800	^{13}C−H stretch
2823			ν_3 ($^{13}CH_3OH$)
2600			$\nu_4 + \nu_{7/11}$ ($^{13}CH_3OH$)
2513			$\nu_6 + \nu_{11}$ ($^{13}CH_3OH$)
2412			$\nu_6 + \nu_7$ ($^{13}CH_3OH$)
	2275		ν_3 ($^{13}CO_2$)
2228			$2\nu_{7/11}$ ($^{13}CH_3OH$)
	2091		ν_1 (^{13}CO)
2004			$2\nu_8$ ($^{13}CH_3OH$)
	1805		ν_2 ($H^{13}CO$)
	1678, 1670, 1590	1689	^{13}C=O stretch
	1569		^{13}C=^{13}C stretch
	1294		ν_4 ($^{13}CH_4$)
1475			ν_4 ($^{13}CH_3OH$)
1459			ν_{10} ($^{13}CH_3OH$)
1415			ν_5 ($^{13}CH_3OH$)
1351			ν_6 ($^{13}CH_3OH$)
	1496		ν_3 (H_2CO)
	1455, 1424, 1400, 1365, 1340, 1260, 1192	1450, 1424, 1372, 1294	^{13}CH bending, $^{13}CH_2$ twisting, O−H bending
1121	1121		ν_7 ($^{13}CH_3OH$)
	1062	1173, 1143	^{13}C−O stretch
1020			ν_{11} ($^{13}CH_3OH$)
1006	1006		ν_8 ($^{13}CH_3OH$)
		794	^{13}C−H wagging
825, 717	829, 720		ν_{12} ($^{13}CH_3OH$)

Table S5. Infrared absorption features of methanol ice ($^{13}CH_3OH$) irradiated at 40 K recorded before irradiation, after irradiation, and after TPD. Assignments based on references (11, 19, 21).

Before irradiation (cm^{-1})	After irradiation (cm^{-1})	After TPD (cm^{-1})	Assignment
	4518		$\nu_2 + \nu_3$ ($^{13}CH_4$)
4378	4390		$\nu_{2/9} + \nu_{4/6/10}$ ($^{13}CH_3OH$)
4267			$\nu_{2/9} + \nu_4$ ($^{13}CH_3OH$)
	4281		$\nu_3 + \nu_4$ ($^{13}CH_4$)
	4192		$2\nu_1$ (^{13}CO)
	4143		$\nu_1 + \nu_4$ ($^{13}CH_4$)
4094			?
3960			$\nu_1 + \nu_{12}$ ($^{13}CH_3OH$)
	3620		$\nu_1 + \nu_{13}$ ($^{13}CO_2$)
	3624, 3500, 3400, 3292, 3195,	3481, 3363, 3211	O−H stretch
3382, 3328, 3276, 3201, 3130			ν_1 ($^{13}CH_3OH$)
2976, 2951			ν_2 ($^{13}CH_3OH$)
2921			ν_9 ($^{13}CH_3OH$)
	2996, 2963, 2933, 2931, 2875, 2836, 2753, 2556	3023, 2960, 2925, 2902, 2866,	^{13}C−H stretch
2825			ν_3 ($^{13}CH_3OH$)
2601			$\nu_4 + \nu_{7/11}$ ($^{13}CH_3OH$)
2513			$\nu_6 + \nu_{11}$ ($^{13}CH_3OH$)
2416			$\nu_6 + \nu_7$ ($^{13}CH_3OH$)
	2275		ν_3 ($^{13}CO_2$)
2226			$2\nu_{7/11}$ ($^{13}CH_3OH$)
	2091		ν_1 (^{13}CO)
2004			$2\nu_8$ ($^{13}CH_3OH$)
	1805		ν_2 ($H^{13}CO$)
	1678, 1674, 1652	1682	^{13}C=O stretch
	1569	1569	^{13}C=^{13}C stretch
	1294		ν_4 ($^{13}CH_4$)
1479			ν_4 ($^{13}CH_3OH$)
1428			ν_{10} ($^{13}CH_3OH$)
1374			ν_5 ($^{13}CH_3OH$)
1348			ν_6 ($^{13}CH_3OH$)
	1496		ν_3 ($H_2{}^{13}CO$)
	1441, 1397, 1265	1441, 1331, 1273, 1223	^{13}CH bending, $^{13}CH_2$ twisting, O−H bending
1124	1124		ν_7 ($^{13}CH_3OH$)
	1068	1091, 966	^{13}C−O stretch
1024			ν_{11} ($^{13}CH_3OH$)
1005	1011		ν_8 ($^{13}CH_3OH$)
	881, 828	869, 841, 803	^{13}C−H wagging/^{13}C−^{13}C−O stretching
822, 724			ν_{12} ($^{13}CH_3OH$)
	639		ν_2 ($^{13}CO_2$)

Table S6. Infrared absorption features of carbon monoxide ice ($^{13}C^{18}O$) irradiated at 10 K recorded before irradiation, after irradiation, and after TPD. Assignments based on references (20-22).

Before irradiation (cm^{-1})	After irradiation (cm^{-1})	After TPD (cm^{-1})	Assignment
4159	4159		$2\nu_1$ (^{13}CO)
4056	4056		$2\nu_1$ ($^{13}C^{18}O$)
	3537		$\nu_1 + \nu_3$ ($^{13}C^{18}O_2$)
	3440		$2\nu_2 + \nu_3$ ($^{13}C^{18}O_2$)
	2938		$\nu_2 + \nu_3$ ($^{13}C_3{}^{18}O_2$)
	2343		$\nu_2 + \nu_4$ ($^{13}C_3{}^{18}O_2$)
	2285		ν_3 ($^{13}CO_2$)
	2264		ν_3 ($^{18}O^{13}CO$)
	2244		ν_3 ($^{13}C^{18}O_2$)
	2153		ν_1 ($^{13}C_3{}^{18}O$)
	2123		ν_3 ($^{13}C_3{}^{18}O_2$)
2107			ν_1 ($C^{17}O$)
2092	2092		ν_1 (^{13}CO)
2065	2065		ν_1 ($^{13}C^{17}O$)
		2180, 2124, 2061	$^{13}C\equiv{}^{13}C$ stretch in conjugated alkynes
2038	2038		ν_1 ($^{13}C^{18}O$)
	2019		ν_2 ($^{13}C_4{}^{18}O_2$)
	1974		$\nu_4 + \nu_6$ ($^{13}C_3{}^{18}O_2$)
	1940		ν_3 ($^{13}C_5{}^{18}O_2$)/ ($^{13}C_6{}^{18}O$)
	1902		ν_3 ($^{13}C_3$)
	1870		ν_4 ($^{13}C_6$)
	1843		ν_1 ($^{13}C_2{}^{18}O$)
	1745		ν_2 ($^{13}C_4{}^{18}O$)
	1708	1708	$^{13}C{=}^{18}O$ stretch
	1639		ν_3 ($^{13}C_5{}^{18}O$)
	671		ν_2 ($^{13}C^{18}O_2$)

Table S7. Infrared absorption features of carbon monoxide ice ($^{13}C^{18}O$) irradiated at 20 K recorded before irradiation, after irradiation, and after TPD. Assignments based on references (20-22).

Before irradiation (cm^{-1})	After irradiation (cm^{-1})	After TPD (cm^{-1})	Assignment
4159	4159		$2\nu_1$ (^{13}CO)
4056	4056		$2\nu_1$ ($^{13}C^{18}O$)
	3537		$\nu_1 + \nu_3$ ($^{13}C^{18}O_2$)
	3440		$2\nu_2 + \nu_3$ ($^{13}C^{18}O_2$)
	2938		$\nu_2 + \nu_3$ ($^{13}C_3{}^{18}O_2$)
	2341		$\nu_2 + \nu_4$ ($^{13}C_3{}^{18}O_2$)
	2286		ν_3 ($^{13}CO_2$)
	2264		ν_3 ($^{18}O^{13}CO$)
	2245		ν_3 ($^{13}C^{18}O_2$)
	2152		ν_1 ($^{13}C_3{}^{18}O$)
	2124		ν_3 ($^{13}C_3{}^{18}O_2$)
2107			ν_1 ($C^{17}O$)
2092	2092		ν_1 (^{13}CO)
2065	2065		ν_1 ($^{13}C^{17}O$)
		2052, 1992	$^{13}C{\equiv}^{13}C$ stretch in conjugated alkynes
2038	2038		ν_1 ($^{13}C^{18}O$)
	2019		ν_2 ($^{13}C_4{}^{18}O_2$)
	1974		$\nu_4 + \nu_6$ ($^{13}C_3{}^{18}O_2$)
	1940		ν_3 ($^{13}C_5{}^{18}O_2$)/ ($^{13}C_6{}^{18}O$)
	1902		ν_3 ($^{13}C_3$)
	1871		ν_4 ($^{13}C_6$)
	1844		ν_1 ($^{13}C_2{}^{18}O$)
	1785		ν_2 ($^{13}C_3{}^{18}O$)
	1746		ν_2 ($^{13}C_4{}^{18}O$)
	1701		$^{13}C{=}^{18}O$ stretch
	1641		ν_3 ($^{13}C_5{}^{18}O$)
	1436		ν_4 ($^{13}C_3{}^{18}O_2$)
	667		ν_2 ($^{13}C^{18}O_2$)

Table S8. Rate constants derived via the solution of the coupled differential equations for the complex reactions in irradiated methanol ices.

Reaction scheme	Rate constant [a] 10 K	Rate constant [a] 40 K
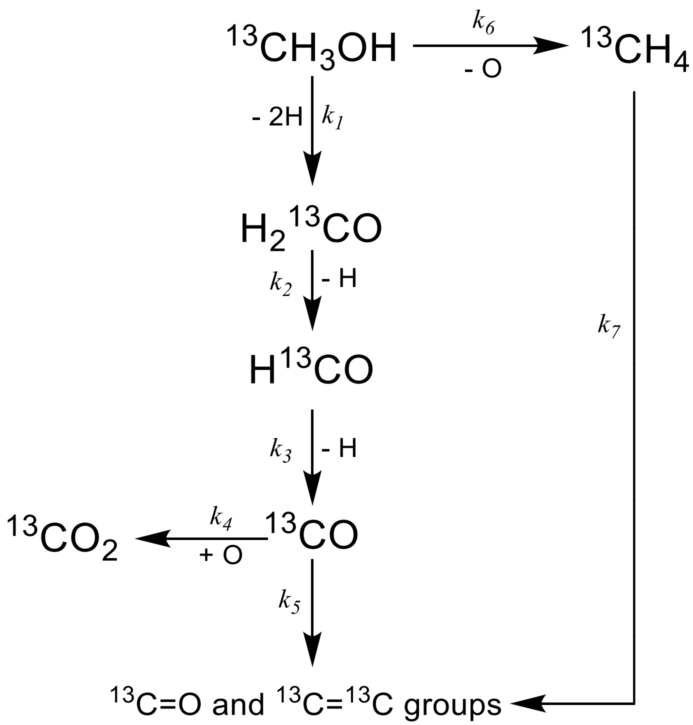	$k_1 = 1.01 \pm 0.36$	$k_1 = 1.07 \pm 0.13$
	$k_2 = 0.81 \pm 0.08$	$k_2 = 0.97 \pm 0.07$
	$k_3 = 0.055 \pm 0.004$	$k_3 = 0.034 \pm 0.002$
	$k_4 = 0.064 \pm 0.004$	$k_4 = 0.050 \pm 0.003$
	$k_5 = 0.20 \pm 0.01$	$k_5 = 0.24 \pm 0.04$
	$k_6 = 0.35 \pm 0.02$	$k_6 = 0.58 \pm 0.03$
	$k_7 = 0.022 \pm 0.004$	$k_7 = 0.0035 \pm 0.004$

[a] The unit is amu eV^{-1}.

Table S9. Rate constants derived via the solution of the coupled differential equations for the complex reactions in irradiated carbon monoxide ices.

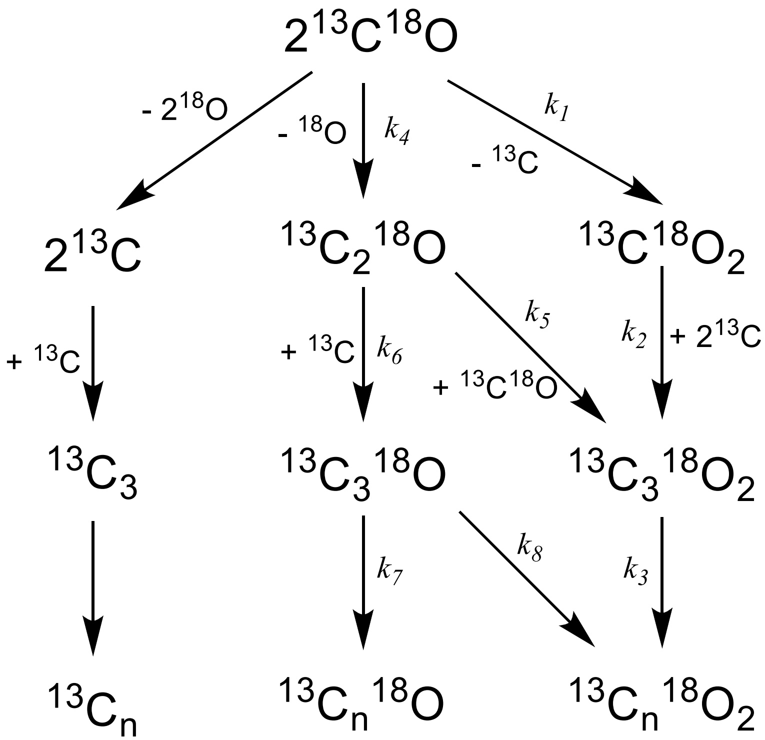

Reaction scheme	Rate constant [a]	
	10 K	20 K
	$k_1 = 0.33 \pm 0.02$	$k_1 = 0.41 \pm 0.05$
	$k_2 = 5.55 \pm 0.11 \times 10^{-6}$	$k_2 = 8.36 \pm 0.06 \times 10^{-6}$
	$k_3 = 0.054 \pm 0.008$	$k_3 = 0.031 \pm 0.004$
	$k_4 = 2.14 \pm 0.08$	$k_4 = 0.11 \pm 0.01$
	$k_5 = 2.41 \pm 0.46$	$k_5 = 4.28 \pm 0.33$
	$k_6 = 22.2 \pm 1.03$	$k_6 = 18.09 \pm 1.15$
	$k_7 = 0.055 \pm 0.003$	$k_7 = 0.0028 \pm 0.0004$
	$k_8 = 0.072 \pm 0.009$	$k_8 = 0.019 \pm 0.005$

[a] The unit is amu eV^{-1}.

Table S10. Concentration (nM) of sugar and sugar-related compounds as BSTFA derivatives in the residue of methanol ice irradiated at 40 K with different doses.

	Compound	^{1}D, ^{2}D RT (min:sec, sec)	Molecular formula	Mass (amu)	Concentration (nM)					
					1.1 eV amu^{-1}	8.8 eV amu^{-1}	23.0 eV amu^{-1}	34.0 eV amu^{-1}	49.3 eV amu^{-1}	82.1 eV amu^{-1}
	Monosaccharides									
1	L-Glyceraldehyde	32:00, 1.004	$^{13}C_3H_6O_3$	93	2080	1573	1733	163	319	nd
	D-Glyceraldehyde	32:39, 0.978	$^{13}C_3H_6O_3$	93	1950	1387	1617	162	280	nd
2	Dihydroxyacetone	42:06, 1.058	$^{13}C_3H_6O_3$	93	110	34	29	5	27	5
3	DL-Erythrose	48:34, 0.869	$^{13}C_4H_8O_4$	124	48	37	71	nd	41	nd
4	DL-Erythrulose	52:07, 0.991	$^{13}C_4H_8O_4$	124	74	38	36	nd	22	nd
5	DL-Arabinose	59:43, 0.811	$^{13}C_5H_{10}O_5$	155	42	5	29	3	11	22
6	DL-Ribose [a]	59:52, 0.779	$^{13}C_5H_{10}O_5$	155	42	8	32	2	16	23
7	DL-Xylose	65:52, 0.861	$^{13}C_5H_{10}O_5$	155	40	7	37	13	21	36
8	DL-Galactose	72:17, 0.826	$^{13}C_6H_{12}O_6$	186	20	4	6	nd	2	2
9	DL-Allose	68:37, 0.738	$^{13}C_6H_{12}O_6$	186	33	3	9	1	3	4
10	DL-Tagatose	71:02, 0.759	$^{13}C_6H_{12}O_6$	186	96	17	37	8	20	25
	Sugar alcohols									
11	DL-Threitol	51:34, 0.741	$^{13}C_4H_{10}O_4$	126	385	54	191	4	65	70
12	Erythritol	51:49, 0.741	$^{13}C_4H_{10}O_4$	126	808	106	310	11	151	164
13	DL-Xylitol	61:58, 0.708	$^{13}C_5H_{12}O_5$	157	278	16	36	1	15	12
14	DL-Arabitol	62:37, 0.709	$^{13}C_5H_{12}O_5$	157	1316	80	126	5	52	51
15	DL-Ribitol	62:52, 0.697	$^{13}C_5H_{12}O_5$	157	414	24	43	2	20	21
16	DL-Mannitol	72:41, 0.754	$^{13}C_6H_{14}O_6$	188	180	30	20	2	10	6
17	DL-Sorbitol	73:08, 0.753	$^{13}C_6H_{14}O_6$	188	58	8	7	nq	3	2
18	Dulcitol	73:23, 0.766	$^{13}C_6H_{14}O_6$	188	75	10	9	nd	4	2
	Sugar acids									
19	DL-Glyceric acid	42:00, 0.908	$^{13}C_3H_6O_4$	109	590	107	183	nd	193	1
20	DL-Erythronic acid	53:46, 0.797	$^{13}C_4H_8O_5$	140	169	28	37	2	35	5
21	DL-Threonic acid	55:07, 0.815	$^{13}C_4H_8O_5$	140	107	16	18	nd	8	nd
	Other sugar related compounds									
22	Glycolic acid	30:30, 0.924	$^{13}C_2H_4O_3$	78	2939	1451	2111	nd	1980	nd
23	Glycolaldehyde	34:48, 1.321	$^{13}C_2H_4O_2$	62	915	223	179	16	110	21

nq = detected but below quantification limit;
nd = not detected.
[a] Concentration values were multiplied by 2 to account for both enantiomers.

Table S11. Prominent positive ion SIMS data from residues of irradiated methanol ($^{13}CH_3OH$).

m/z	Representative formula	Representative structures (all carbon atoms are ^{13}C)
16.0268	$^{13}CH_3$	$CH_3^{\oplus}$
29.0302	$^{13}C_2H_3$	$H_2C{=}CH^{\oplus}$
31.0459	$^{13}C_2H_5$	$H_3C{-}CH_2^{\oplus}$
32.0218	$^{13}CH_3O$	$HO{-}CH_2^{\oplus}$
42.0336	$^{13}C_3H_3$	$H_2C{=}C{=}CH^{\oplus}$
44.0492	$^{13}C_3H_5$	$H_2C{=}CH{-}CH_2^{\oplus}$
45.0251	$^{13}C_2H_3O$	$HO{-}HC{=}CH^{\oplus}$
47.0408	$^{13}C_2H_5O$	$HO{-}H_2C{-}CH_2^{\oplus}$
57.0526	$^{13}C_4H_5$	$HC{\equiv}C{-}H_2C{-}CH_2^{\oplus}$
58.0285	$^{13}C_3H_3O$	$HO{-}HC{=}C{=}CH^{\oplus}$
59.0683	$^{13}C_4H_7$	$H_2C{=}HC{-}H_2C{-}CH_2^{\oplus}$
60.0442	$^{13}C_3H_5O$	$HO{-}H_2C{-}HC{=}CH^{\oplus}$
72.0716	$^{13}C_5H_7$	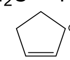
73.0475	$^{13}C_4H_5O$	$HO{-}H_2C{-}HC{=}C{=}CH^{\oplus}$
74.0234	$^{13}C_3H_3O_2$	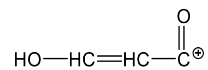
75.0632	$^{13}C_4H_7O$	$HO{-}H_2C{-}H_2C{-}HC{=}CH^{\oplus}$
76.0391	$^{13}C_3H_5O_2$	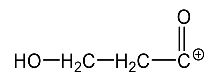
83.0593	$^{13}C_6H_5$	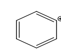
88.0665	$^{13}C_5H_7O$	$HO{-}H_2C{-}H_2C{-}HC{=}C{=}CH^{\oplus}$
89.0424	$^{13}C_4H_5O_2$	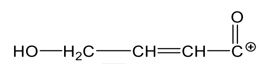
98.0783	$^{13}C_7H_7$	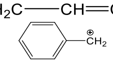
102.058	$^{13}C_5H_5O_2$	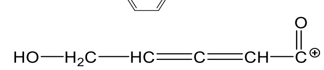
113.0974	$^{13}C_8H_9$	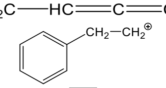
114.0732	$^{13}C_7H_7O$	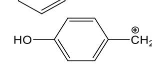
117.0648	$^{13}C_6H_7O_2$	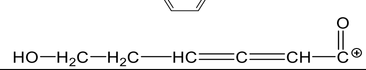

Table S11. *continued*

124.085	$^{13}C_9H_7$	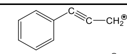
130.132	$^{13}C_8H_{10}O$	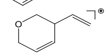
138.0962	$^{13}C_{10}H_8$	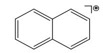
152.1074	$^{13}C_{11}H_9$	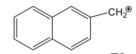
164.103	$^{13}C_{12}H_8$	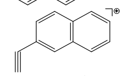
178.1142	$^{13}C_{13}H_9$	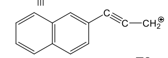
192.1253	$^{13}C_{14}H_{10}$	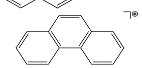
204.1209	$^{13}C_{15}H_9$	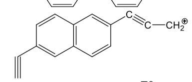
218.1312	$^{13}C_{16}H_{10}$	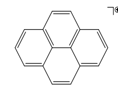
232.1432	$^{13}C_{17}H_{11}$	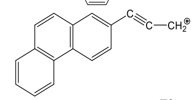
244.1388	$^{13}C_{18}H_{10}$	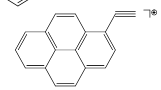
258.15	$^{13}C_{19}H_{11}$	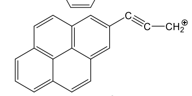
272.1612	$^{13}C_{20}H_{12}$	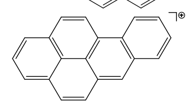 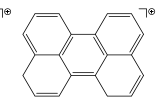
284.1567	$^{13}C_{21}H_{11}$	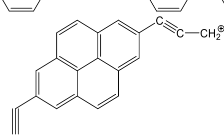
298.1679	$^{13}C_{22}H_{12}$	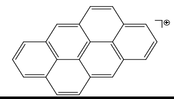 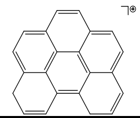

Table S12. Prominent negative ion SIMS data from residues of irradiated methanol ($^{13}CH_3OH$).

m/z	Representative formula	Representative structures (all carbon atoms are ^{13}C)
14.0112	^{13}CH	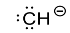
15.9942	O	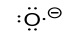
17.0028	OH	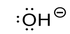
27.0146	$^{13}C_2H$	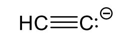
43.0095	$^{13}C_2HO$	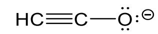
45.0251	$^{13}C_2H_3O$	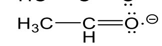
46.001	$^{13}CHO_2$	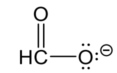
53.0213	$^{13}C_4H$	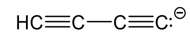
61.02	$^{13}C_2H_3O_2$	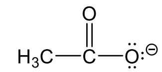
69.0162	$^{13}C_4HO$	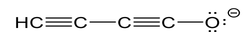
74.0234	$^{13}C_3H_3O_2$	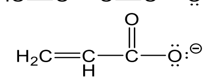
79.028	$^{13}C_6H$	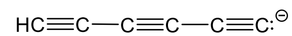
89.0424	$^{13}C_4H_5O_2$	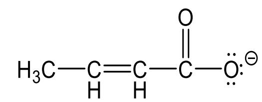
90.0183	$^{13}C_3H_3O_3$	
99.0542	$^{13}C_6H_5O$	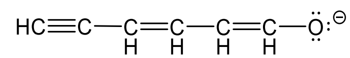
105.0347	$^{13}C_8H$/$^{13}C_4H_5O_3$	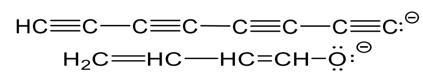
118.0381	$^{13}C_9H$	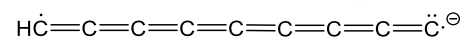
131.0414	$^{13}C_{10}H$	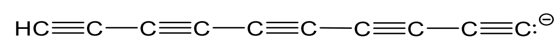

Table S13. Prominent positive ion SIMS data from residues of irradiated carbon monoxide ($^{13}C^{18}O$).

m/z	Representative formula	Representative structures (all carbon atoms are ^{13}C)
15.019	$^{13}CH_2$	$\dot{C}H_2^{\oplus}$
27.0146	$^{13}C_2H$	$HC{\equiv}C^{\oplus}$
30.038	$^{13}C_2H_4$	$H_3C{-}\dot{C}H^{\oplus}$
41.0257	$^{13}C_3H_2$	$HC{\equiv}C{-}\dot{C}H^{\oplus}$
43.0414	$^{13}C_3H_4$	$H_2C{=}HC{-}\dot{C}H^{\oplus}$
55.0369	$^{13}C_4H_3$	$HC{\equiv}C{-}CH{=}CH^{\oplus}$
67.0325	$^{13}C_5H_2$	$H\dot{C}{=}C{=}C{=}C{=}CH^{\oplus}$
81.0554	$^{13}C_3H_6{}^{18}O_2$	$HO{-}CH_2{-}CH_2{-}\dot{C}(OH)^{\oplus}$
93.0392	$^{13}C_7H_2$	$H\dot{C}{=}C{=}C{=}C{=}C{=}C{=}CH^{\oplus}$
106.0425	$^{13}C_8H_2$	$HC{\equiv}C{-}C{\equiv}C{-}C{\equiv}C{-}\dot{C}{=}CH^{\oplus}$
119.0459	$^{13}C_9H_2$	$H\dot{C}{=}C{=}C{=}C{=}C{=}C{=}C{=}C{=}CH^{\oplus}$
132.0493	$^{13}C_{10}H_2$	$HC{\equiv}C{-}C{\equiv}C{-}C{\equiv}C{-}C{\equiv}C{-}\dot{C}{=}CH^{\oplus}$
145.0526	$^{13}C_{11}H_2$	$H\dot{C}{=}C{=}C{=}C{=}C{=}C{=}C{=}C{=}C{=}C{=}CH^{\oplus}$
158.056	$^{13}C_{12}H_2$	$HC{\equiv}C{-}C{\equiv}C{-}C{\equiv}C{-}C{\equiv}C{-}C{\equiv}C{-}\dot{C}{=}CH^{\oplus}$
171.0593	$^{13}C_{13}H_2$	$H\dot{C}{=}C{=}C{=}C{=}C{=}C{=}C{=}C{=}C{=}C{=}C{=}C{=}CH^{\oplus}$
184.0627	$^{13}C_{14}H_2$	$HC{\equiv}C{-}C{\equiv}C{-}C{\equiv}C{-}C{\equiv}C{-}C{\equiv}C{-}C{\equiv}C{-}\dot{C}{=}CH^{\oplus}$

Table S14. Prominent negative ion SIMS data from residues of irradiated carbon monoxide ($^{13}C^{18}O$).

m/z	Representative formula	Representative structures (all carbon atoms are ^{13}C)
17.992	^{18}O	$:\underset{\cdot\cdot}{\ddot{O}}\cdot^{\ominus}$
27.0146	$^{13}C_2H$	$HC\equiv\ddot{C}^{\ominus}$
45.0137	$^{13}C_2{}^{18}OH$	$HO-C\equiv\ddot{C}^{\ominus}$
53.0213	$^{13}C_4H$	$HC\equiv C-C\equiv\ddot{C}^{\ominus}$
71.0204	$^{13}C_4{}^{18}OH$	$HO-C\equiv C-C\equiv\ddot{C}^{\ominus}$
79.028	$^{13}C_6H$	$HC\equiv C-C\equiv C-C\equiv\ddot{C}^{\ominus}$
97.0272	$^{13}C_6{}^{18}OH$	$HO-C\equiv C-C\equiv C-C\equiv\ddot{C}^{\ominus}$
105.0347	$^{13}C_8H$	$HC\equiv C-C\equiv C-C\equiv C-C\equiv\ddot{C}^{\ominus}$
131.0121	$^{13}C_{10}H$	$HC\equiv C-C\equiv C-C\equiv C-C\equiv C-C\equiv\ddot{C}^{\ominus}$
157.0482	$^{13}C_{12}H$	$HC\equiv C-C\equiv C-C\equiv C-C\equiv C-C\equiv C-C\equiv\ddot{C}^{\ominus}$
170.0515	$^{13}C_{13}H$	$H\dot{C}=C=C=C=C=C=C=C=C=C=C=C=\dot{C}^{\oplus}$
183.0256	$^{13}C_{14}H$	$HC\equiv C-C\equiv C-C\equiv C-C\equiv C-C\equiv C-C\equiv C-C\equiv\ddot{C}^{\ominus}$

SI Reference:

1. J. M. Hollis, F. J. Lovas, P. R. Jewell, Interstellar Glycolaldehyde: The First Sugar. *Astrophys. J.* **540**, L107−L110 (2000).
2. S. Maity, R. I. Kaiser, B. M. Jones, Formation of complex organic molecules in methanol and methanol-carbon monoxide ices exposed to ionizing radiation--a combined FTIR and reflectron time-of-flight mass spectrometry study. *Phys. Chem. Chem. Phys.* **17**, 3081−3114 (2015).
3. C. J. Bennett, R. I. Kaiser, On the Formation of Glycolaldehyde ($HCOCH_2OH$) and Methyl Formate ($HCOOCH_3$) in Interstellar Ice Analogs. *Astrophys. J.* **661**, 899−909 (2007).
4. P. de Marcellus *et al.*, Aldehydes and sugars from evolved precometary ice analogs: importance of ices in astrochemical and prebiotic evolution. *Proc. Natl. Acad. Sci. USA* **112**, 965−970 (2015).
5. C. Meinert *et al.*, Ribose and related sugars from ultraviolet irradiation of interstellar ice analogs. *Science* **352**, 208−212 (2016).
6. Y. Furukawa *et al.*, Extraterrestrial ribose and other sugars in primitive meteorites. *Proc. Natl. Acad. Sci. USA* **116**, 24440−24445 (2019).
7. M. Nuevo, G. Cooper, S. A. Sandford, Deoxyribose and deoxysugar derivatives from photoprocessed astrophysical ice analogues and comparison to meteorites. *Nat. Commun.* **9**, 5276 (2018).
8. G. Cooper, A. C. Rios, Enantiomer excesses of rare and common sugar derivatives in carbonaceous meteorites. *Proc. Natl. Acad. Sci. USA* **113**, E3322−E3331 (2016).
9. J. M. Hollis, F. J. Lovas, P. R. Jewell, L. H. Coudert, Interstellar Antifreeze: Ethylene Glycol. *Astrophys. J.* **571**, L59−L62 (2002).
10. F. Schmidt, P. Swiderek, J. H. Bredehöft, Electron-Induced Processing of Methanol Ice. *ACS Earth Space Chem.* **5**, 391−408 (2021).
11. C. Zhu, A. M. Turner, C. Meinert, R. I. Kaiser, On the Production of Polyols and Hydroxycarboxylic Acids in Interstellar Analogous Ices of Methanol. *Astrophys. J.* **889**, 134 (2020).
12. K. K. Sullivan *et al.*, Low-energy (<20 eV) and high-energy (1000 eV) electron-induced methanol radiolysis of astrochemical interest. *Mon. Not. R. Astron. Soc.* **460**, 664−672 (2016).
13. D. M. Paardekooper, J. B. Bossa, H. Linnartz, Laser desorption time-of-flight mass spectrometry of vacuum UV photo-processed methanol ice. *Astron. Astrophys.* **592**, A67 (2016).

14. A. A. Monroe, S. Pizzarello, The soluble organic compounds of the Bells meteorite: Not a unique or unusual composition. *Geochim. Cosmochim. Acta* **75**, 7585−7595 (2011).
15. G. Cooper *et al.*, Carbonaceous meteorites as a source of sugar-related organic compounds for the early Earth. *Nature* **414**, 879−883 (2001).
16. R. I. Kaiser, S. Maity, B. M. Jones, Synthesis of prebiotic glycerol in interstellar ices. *Angew. Chem. Int. Ed. Engl.* **54**, 195−200 (2015).
17. J. H. Marks *et al.*, Complex Reactive Acids from Methanol and Carbon Dioxide Ice: Glycolic Acid ($HOCH_2COOH$) and Carbonic Acid Monomethyl Ester (CH_3OCOOH). *Astrophys. J.* **942**, 43 (2023).
18. M. Bouilloud *et al.*, Bibliographic review and new measurements of the infrared band strengths of pure molecules at 25 K: H_2O, CO_2, CO, CH_4, NH_3, CH_3OH, HCOOH and H_2CO. *Mon. Not. R. Astron. Soc.* **451**, 2145−2160 (2015).
19. C. J. Bennett, S.-H. Chen, B.-J. Sun, A. H. H. Chang, R. I. Kaiser, Mechanistical Studies on the Irradiation of Methanol in Extraterrestrial Ices. *Astrophys. J.* **660**, 1588−1608 (2007).
20. C. S. Jamieson, A. M. Mebel, R. I. Kaiser, Understanding the Kinetics and Dynamics of Radiation-induced Reaction Pathways in Carbon Monoxide Ice at 10 K. *Astrophys. J., Suppl. Ser.* **163**, 184−206 (2006).
21. G. Socrates, *Infrared and Raman Characteristic Group Frequencies: Tables and Charts* (Wiley, Chichester, ed. 3rd, 2004).
22. C. J. Bennett, C. S. Jamieson, R. I. Kaiser, Mechanistical studies on the formation of carbon dioxide in extraterrestrial carbon monoxide ice analog samples. *Phys. Chem. Chem. Phys.* **11**, 4210−4218 (2009).